CHAPTER

13

Scintillators

FRANK WILKINSON III
Alpha Spectra, Inc. Grand Junction, Colorado

"Ex luce lucellum."—*Robert Lowe*

I. INTRODUCTION

In 1948, Robert Hofstadter first described the use of the alkali halide crystal, NaI(Tl), as a scintillation detector. His first measurements with NaI(Tl) used 8 g of powder that contained crystals that were only 1–2 mm on a side (Hofstadter, 1948). In 1978, the technology had advanced to the point where Hofstadter and his collaborators (Crystal Ball Collaboration, 1980), along with a design team from The Harshaw Chemical Company, built the Crystal Ball detector that consisted of over 4 million g of NaI(Tl) material. The Crystal Ball was used at the positron-electron ring of the Stanford Linear Accelerator Center to investigate the building blocks that make up electrons and positrons.

Since the 1950s, scintillators of various materials have been used in diverse applications from investigating the smallest particles known to scientists to exploring the origins and the extent of the universe. Detectors have been used for oil, gas, and precious-mineral exploration; health physics; industrial gauges; and nuclear power plant applications. Government labs including the Department of Defense, the Department of Energy, and the Environmental Protection Agency use scintillation detectors. These are only a few of the many different and fascinating applications for scintillators in industry, medicine, government research, and academic research. One of the world's largest consumers of scintillation materials is the medical-imaging marketplace. New scintillation-detector configurations are continually being developed and tested in an effort to provide better diagnostic care for the patient.

The characteristics and physical properties of inorganic scintillators are presented in this chapter. The mechanism for the scintillation process is reviewed, and detector design issues are presented. Crystal growth issues and detector manufacturing methods are discussed, and a review of a typical scintillation counting system is presented. The chapter concludes with a brief discussion of the use of scintillators in medical imaging. Scintillators have been used in many different modes and applications; the discussion here is limited to their use in detecting X-rays and gamma-rays.

II. GAMMA-RAY INTERACTIONS IN SCINTILLATION CRYSTALS

The nuclear decay process of some isotopes can include the emission of photons called gamma-rays. Gamma-rays

TABLE 1 Radio Isotopes Useful in Medical Imaging Technology

Isotope	Half-Life ($t_{1/2}$)	Gamma Energies (keV)[a]	Application and Notes
^{57}Co	271 days	122 (86), 136 (11)	Calibration and test positron emitter
^{137}Cs	30 years	662 keV of Ba-137^{m} (90)	Specifications, calibration, and testing
^{18}F	1.8 h	—	Clinical positron emitter
^{99m}Tc	6.0 h	140 (89)	Clinical gamma emitter
^{201}Tl	3.0 days	167 (11), 135 (3)	Clinical emitter
^{67}Ga	3.3 days	93 (37), 184 (20)	Clinical emitter
^{111}In	2.8 days	245 (94), 172 (90)	Clinical emitter
^{123}I	13.2 h	159 (83), 529 (14)	Clinical emitter
^{22}Na	2.6 years	1567 (100)	Calibration and test positron emitter
^{40}K	1.26×10^9 years	1461 (11)	Naturally occurring

are part of the electromagnetic spectrum. In a vacuum, these photons travel at the speed of light, 3×10^{10} cm/s. Gamma-ray energies are typically in the range of a few thousand electron volts to many million electron volts, whereas X-rays have energy less than 100 keV. Table 1 gives useful information about several radioisotopes relevant to medical imaging.

In order to understand the scintillation process and how scintillators detect gamma radiation, it is important to understand how gamma-rays interact with matter. Because the typical gamma-ray energy is greater than the average binding energy of an electron, gamma-rays have enough energy to ionize matter. There are three important mechanisms for interaction: the photoelectric effect, Compton scattering, and pair production. In each of these physical processes, the photon incident on the crystal gives up all or part of its energy to the electrons in the crystalline matrix.

A. The Photoelectric Process

In the photoelectric process, the incident photon gives up all of its energy to a bound electron. The incident photon is completely absorbed by a photoelectron. The photoelectron kinetic energy is given by:

$$E_{e^-} = h\nu - E_b \quad (1)$$

where $h\nu$ represents the photon's energy and E_b is the binding energy of the bound electron before it leaves its atomic shell. In a metal, and other crystalline structures, this second term is the familiar work function of the material. The photoelectric process requires that the electron absorbing the energy be in close proximity to an atom. Effectively, it must be a bound electron in order to ensure that conservation of energy and momentum are satisfied during the interaction. Here, the recoil of the atom left behind conserves momentum, whereas Eq. (1) conserves energy. Figure 1 demonstrates this interaction schematically.

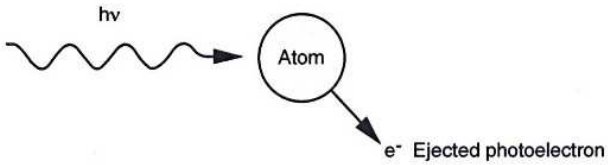

FIGURE 1 The photoelectric effect.

The likelihood that a photon is absorbed is strongly related to the atomic number of the nucleus. The probability of a reaction increases approximately as Z^4, where Z is the atomic number. It follows that a good scintillator will have a high atomic number.

After the electron is ejected from the atom, a vacancy exists in the atomic structure because the electron has absorbed the photon energy. The newly created atomic structure, or positively charged ion, will remain in an excited state for a short time. An electron from a higher energy level will fill the hole in the atomic structure in order to bring the atom to its lowest energy state. A photon is released when the electron moves from a higher energy state to the lower energy state. The released photon energy is exactly the energy difference between the initial and the final states of the electron; this photon is called a *characteristic X-ray*. The electron transition occurs in the crystalline lattice in approximately 1 ns.

The reabsorption of the X-ray energy by another atomic electron in an outer shell often occurs before the X-ray can leave the atom. This electron, called an *Auger electron*, has enough translational energy to leave the atom. Electrons from the outer shells will fill the two vacancies, causing the emission of additional characteristic X-rays and possibly Auger electrons.

The sharp rise in the mass attenuation coefficient at 32 keV (shown in Fig. 2) is equal to the binding energy of the K-shell electron in iodine. The structure in the curve

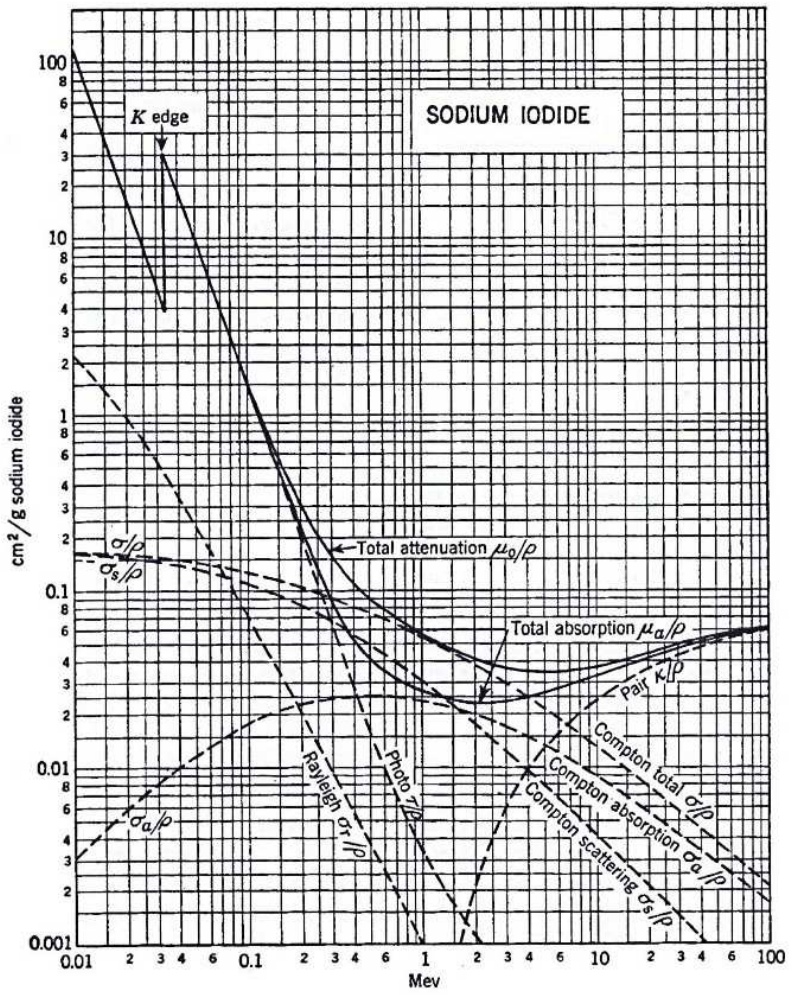

FIGURE 2 Mass attenuation coefficient curves for NaI(Tl). (From Evans, R.D. "The Atomic Nucleus." Krieger Publishing, Melbourne, FL, with permission.)

seen at 32 keV is an absorption edge. The characteristic X-ray emitted is usually reabsorbed by another atom near the initial event. When all the initial photon energy stays in the crystal, the total electron kinetic energy must be equal to the total energy of the incident photon. Ideally, the photoelectric events produced in the crystal are represented as a delta function in the gamma-ray spectrum (see Fig. 3).

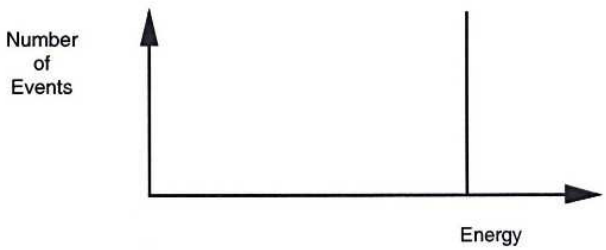

FIGURE 3 Ideal photopeak response.

B. The Compton Effect

In some cases, a photon enters the crystal lattice and scatters off an electron. The scattered photon and the electron will share the energy of the incident photon. Figure 4 shows a diagram of such a scattering event. The scattered photon energy, $h\nu'$, can be expressed in terms of the initial photon energy $h\nu$, the rest mass energy of the electron m_0c^2, and the photon scattering angle θ:

$$h\nu' = \frac{h\nu}{1+(h\nu/m_0c^2)(1-\cos\theta)} \tag{2}$$

This expression is derived by conserving energy and momentum in a classical two-body collision and by using the relativistic relationships between momentum and total

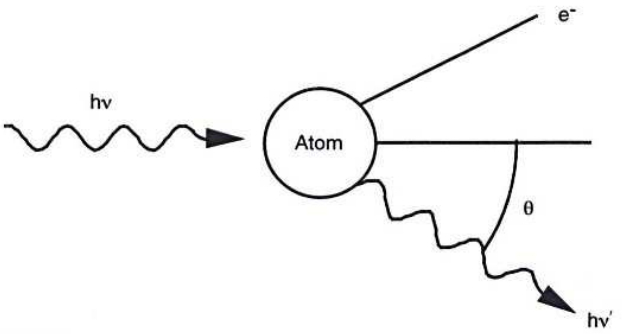

FIGURE 4 Scattering event diagram.

energy (Evans, 1955). In the case of the head-on collision, when $\theta \cong 180°$, the maximum amount of energy is transferred to the electron and the photon shows up in the lower end of the energy distribution (see Fig. 5). In the case of a negligible interaction, when $\theta \cong 0°$, a minimal amount of energy is transferred to an electron; these events represent the photons that are at the higher end of the Compton spectrum. The sharp edge at photon energies corresponding to $\theta \cong 0°$, when observed in a gamma-ray spectrum, is called the *Compton shoulder*. Figure 6 is a plot showing the scattering angle *vs*, the ratio of $h\nu$ to $h\nu'$ for several gamma-ray energies. The figure demonstrates that for very small angles ($\theta \cong 0°$) there is very little energy lost by the incident photon, whereas at larger scattering angles ($\theta \cong 180°$) the incident photon loses much more energy. Remember that the scattered photon while still in the crystal, is available for additional scattering events and possibly a final photoelectric event. When all the initial photon energy is deposited in the crystal, the sum total of all events related to the initial incident photon will show up in the measurement system as a full energy event and will be indistinguishable from photoelectric events.

The energy of the scattered electron is given by:

$$E_{e^-} = h\nu - h\nu' \tag{3}$$

By substituting Eq. (3) into Eq. (2), we obtain:

$$E_{e^-} = \frac{(h\nu)(h\nu / m_0c^2)(1-\cos\theta)}{1+(h\nu / m_0c^2)(1-\cos\theta)} \tag{4}$$

Equation (2) predicts the scattered photon energy; Eq. (4) predicts the kinetic energy of the electron for a given photon-scattering angle. The angular distribution of the scattered gamma-rays is obtained from the *Klein-Nishina formula*, which is written in terms of the differential scattering cross section:

$$\frac{d\sigma}{d\Omega} = Zr_0{}^2\left[\frac{1}{1+\alpha(1-\cos\theta)}\right]^2\left(\frac{1+\cos^2\theta}{2}\right) \left\{1+\frac{\alpha^2(1-\cos\theta)^2}{(1+\cos^2\theta)[1+\alpha(1-\cos\theta)]}\right\} \tag{5}$$

where Z is the atomic number, α is the familiar term $h\nu/m_0c^2$, and r_0 is the classic electron radius. This expression gives us the probability that a photon will be scattered through a given angle in terms of the photon energy, the electron density, and the photon-scattering angle. Because the expression is derived as the probability for an interaction with an electron, the probability is given in unit area per number of photons. A polar plot of the scattering probability for several medical-imaging photon energies is shown in Figure 7. The greater the incident photon energy, the more likely that the photon will preferentially be scattered in the forward direction. Also, note that as the electron density increases in Eq. (5) with the Z of the material, the probability for a scattering interaction through a given angle increases linearly. Here, the amplitude factor Z_0r^2 is set to unity. Scintillation detector materials and detector designs are influenced by the parameters discussed here.

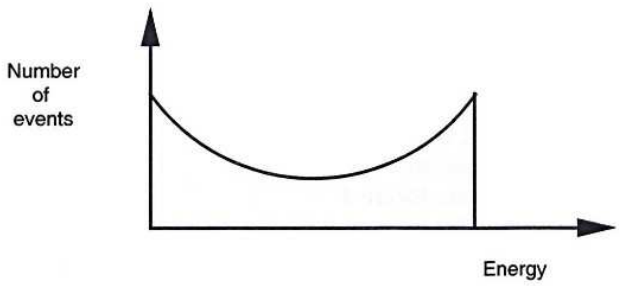

FIGURE 5 Ideal Compton scattering response function.

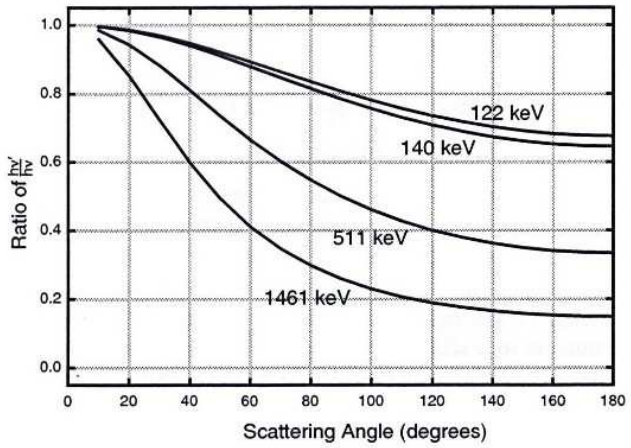

FIGURE 6 Ratio of scattered photon energy to incident photon energy (normalized) plotted against scattering angle.

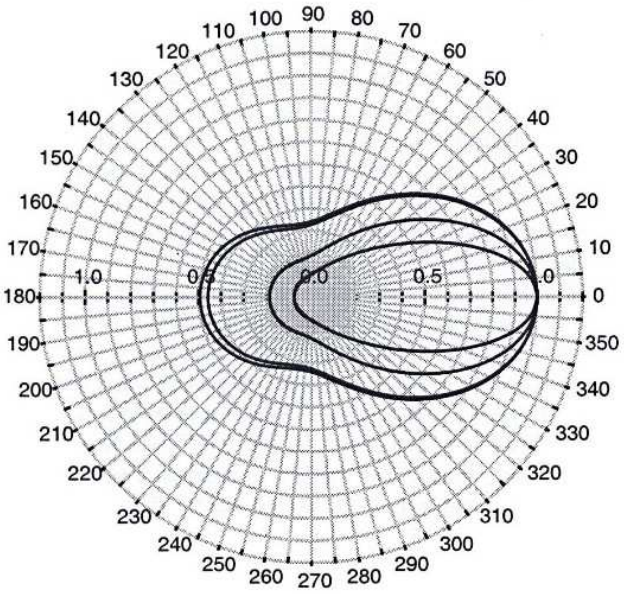

FIGURE 7 Klein-Nishina polar plot. The incident photon is approaching on axis from $\theta = 180°$.

C. Pair Production

In the case in which the incident photon energy exceeds two times the rest mass energy of the electron, pair production can occur; an electron and a positron appear in place of the incident photon. This process must occur in the Coulomb field of a nucleus in order to conserve momentum. Energy is conserved by:

$$E_{e^-} + E_{e^+} = h\nu - 2m_0c^2 \tag{6}$$

This event is shown schematically in Figure 8. The angular distribution of the created electron-positron pair is predominantly forward for high-energy photons. The positron quickly

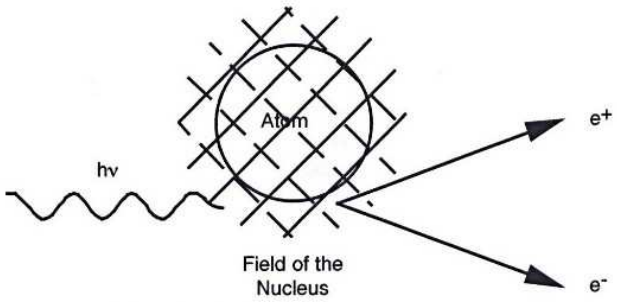

FIGURE 8 Pair production diagram.

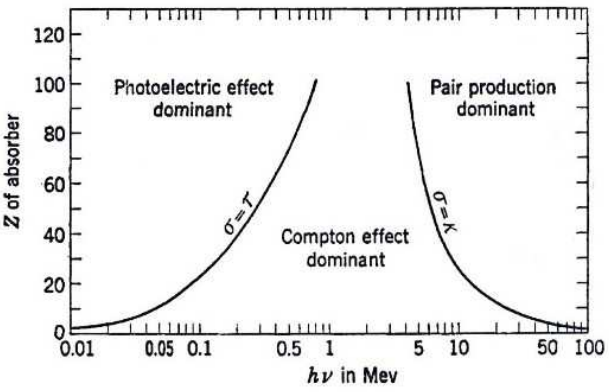

FIGURE 9 Three interaction mechanisms. (From Evans, R.D. "The Atomic Nucleus." Krieger Publishing, Melbourne, FL, with permission.)

recombines with any available electron, causing the creation of two 511 keV photons, which are emitted in coincidence and 180° apart. This process is called *positron annihilation*. This effect can cause some interesting effects on the observed gamma-ray spectrum. If one of the 511-keV photons escapes the crystal, then we observe additional peak in the gamma-ray spectrum at the full-energy photopeak minus 511 keV. We can observe another escape photo peak two times 511 keV. Having some knowledge of the radioisotopes present during a measurement reduces our confusion when interpreting a gamma-ray spectrum.

Whereas Figure 2 gives the mass attenuation coefficients for NaI(Tl), Figure 9 shows the incident photon energy with the Z of the material and plots the curve in which the interaction probability, or cross section, for each adjacent effect is equal. The figure demonstrates the regions in which the three interaction mechanisms dominate. Both figures demonstrate the strong dependence on the incident photon energy.

III. THE CHARACTERISTICS AND PHYSICAL PROPERTIES OF SCINTILLATORS

In this section, we first consider the properties that an ideal scintillator might possess. Knowledge of material properties

is crucial in determining the appropriate material that will provide the needed performance for a given application.

The ideal scintillation detector material should convert all the incident photon energy into scintillation pulses. The photoconversion should respond linearly as a function of energy. Its light output should be maximized in order to optimize the detector's energy resolution. And the emission wavelength of the scintillator's light should match well with the response wavelength of commercially available photosensitive devices.

An ideal scintillation detector should have good stopping power; consequently a material that has high density and high-Z material would be beneficial. High count-rate applications and fast sampling rates require that the ideal crystal's light emission pulse have a fast rise time and fast decay time with no afterglow. This characteristic effectively removes signal pulse pile-up during electronic signal processing. At the same time, the material should be easy to grow in large volumes to meet the needs of any conceivable application. The ideal material should be nonhygroscopic, making the material easier to handle during manufacturing. The ideal material should be mechanically rugged so that it can withstand both mechanical and thermal shock. The index of refraction should be close to that of glass ($n \cong 1.5$) so that no light loss will occur when coupling the crystal to a photosensitive device. The crystal should have high optical light transmission and no self-absorption. The crystal should perform with a good signal-to-noise ratio and with no intrinsic radioactive background.

In reality, no scintillator behaves as the ideal scintillator described here. The selection of any scintillation material for a specific application entails a compromise in which some properties are optimized and other properties are diminished. NaI(Tl) is the scintillation material that comes closest to meeting most of these requirements; consequently, it is the most widely used.

A. Light Output

The intrinsic physical properties of the scintillating material determine its ability to produce light efficiently. Lempicki *et al.* (1999) discuss three significant quantities that determine a material's potential to have good light output: conversion efficiency, transfer efficiency, and luminescence efficiency. Each parameter influences the number of useful photons created per incident amount of photon energy deposited in the crystal. A detailed presentation of these parameters and how each affects the process of light emission can quickly become very complicated; a more detailed investigation is left to the reader (Rodnyi, 1997; Derenzo *et al.*, 1999).

For the purpose of this discussion, the amount of light that exits the crystal at the interface with the photosensitive device is called the *functional light output*. The functional light output is influenced by the detector design and by the assembly techniques used during the encapsulation of the crystal into the final detector assembly. These detector fabrication issues are discussed in a later section.

1. Luminescence in a Scintillator

Converting gamma-ray energy into useful light pulses can be described using a simple solid-state model that illustrates the band structure of an inorganic scintillator. Birks (1964) and Rodnyi (1997) give good presentations of this model of a scintillator. Figure 10 illustrates the band-gap structure in a scintillation crystal. The filled band represents the lower allowed energy levels that are usually occupied by electrons. The valence band is the highest filled band-gap and is made up of electrons that are effectively bound to the crystalline lattice sites. The conduction band contains mobile electrons after an ionizing event occurs in the scintillator. According to Schrödinger's equation, electrons can only exist in discrete energy levels; consequently, regions called forbidden gaps are essential to the model. In a pure crystal, no electrons would be found in these forbidden gaps.

The energy deposited in the lattice by a gamma-ray creates electron-hole pairs. For every electron that moves into a higher energy level in the conduction band a hole is created in the valence band. The number of electron-hole pairs created per unit of energy deposited by the photon is called the *conversion efficiency*.

When a single electron moves from the conduction band and returns to the valence band, the result is a visible light photon that has energy slightly less than that of the band-gap. A characteristic X-ray emission occurs when electrons move from the higher energy-filled bands to a hole in the lower core bands (not shown in Fig. 10). These X-rays have more energy than visible photon emissions. They are typically reabsorbed within the crystal before they can escape

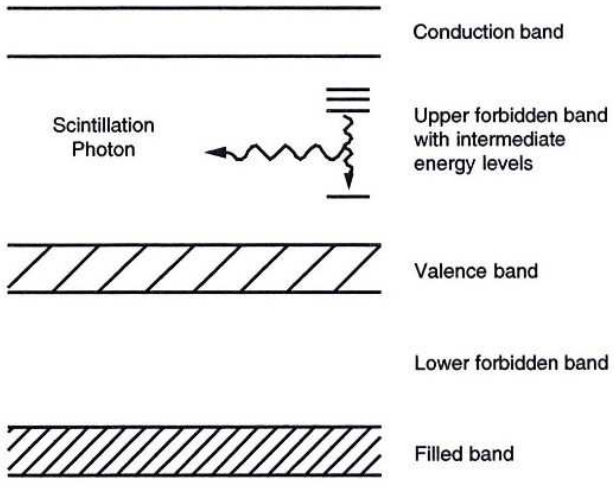

FIGURE 10 Solid-state model showing energy level bands in a scintillator.

and are available to be reabsorbed as part of the total integrated scintillation event in the crystal.

Impurities or lattice defects called *activators* are intentionally introduced into the crystalline lattice so that additional intermediate energy states are created in the forbidden band gap, becoming localized sites throughout the upper forbidden band gap. These defects, called *luminescence centers*, increase electron mobility by shifting the band-gap width enough to put the wavelength of the emitted photons into the visible region of the electromagnetic spectrum. The fractional amount of electron-hole energy that is transferred to the luminescence center is called the *transfer efficiency*. Ideally, transfer energy losses are zero; however, in reality some of the energy loss does occur when the holes or electrons migrate through the lattice or when electron-hole pairs recombine nonradiatively. The efficient transfer of electron energy in the luminescence center requires that holes in the valence band be readily available for recombination with electrons that are trapped in an activation center. If hole mobility is limited, the scintillation rise time will be slow. *Photoluminescence* occurs when photons with energies of less than 6 eV directly excite an activation center.

When a scintillator emits light after absorbing photons, this is called *luminescence*. The amount of thermal energy available in the material affects the luminescent efficiency or luminescent quantum efficiency. Consider the discrete levels present in the crystal lattice. The energy levels of the activation centers are influenced by the amount of thermal energy present in the crystalline lattice; as thermal energy is absorbed by the crystalline lattice, a shift from the equilibrium quantum states results. The result is that nonradiative transitions can occur by heat dissipation rather than by emitting radiation. This effect is called thermal quenching.

Each scintillation material has unique band gaps and activation centers with well-defined energy differences. The electronic transitions that occur between the energy states in the activation center dictate the wavelengths of the light emitted by the crystal. Accordingly, the model explains why we observe that each scintillator material has its own characteristic light emission curve. Good scintillators have emission band gaps that do not overlap with the optical absorption band gaps because an overlap causes the excessive self-absorption of light in the crystal.

Scintillators generate light over a wide range of wavelengths of the visible spectrum. As seen in Table 2, CsF emits in the ultraviolet region ($\lambda \cong 390$ nm), NaI(Tl) emits blue light ($\lambda \cong 415$ nm) at its maximum, and CsI(Tl) emits green light ($\lambda \cong 540$ nm) at its maximum.

The model presented here is specific to crystals that require an activator. These crystals are called *extrinsic scintillators*; examples are NaI(Tl), CsI(Tl), and LSO(Ce). Some crystal materials do not require a dopant to efficiently give off light; they are called *intrinsic scintillators*; examples are BGO, $CdWO_4$, and BaF_2. There are several clear advantages to some of the intrinsic scintillators, including typically higher radiation hardness, avoiding the

TABLE 2 Properties of the Common Scintillation Detector Crystal Materials[a]

Material[b]	Density (g/cm^3)	Effective Atomic Number, Z_{eff}	Wavelength of Maximum Emission (nm)	Principal Decay Constant (μs)[c]	Pulse Rise Time (ps)	Index of Refraction at Emission Maximum, n	Hygroscopic
NaI(Tl)	3.67	51	415	0.23	—	1.85	Yes
$Bi_4Ge_3O_{12}$	7.13	76	505	0.30	30 ± 30	2.15	No
CsI(Na)	4:51	54	420	0.63	—	1.84	Slightly
CsI(Tl)[d]	4.51	54	540	0.68	9500, 41000	1.80	Slightly
Lu_2SiO_5(Ce)	7.40	65	420	0.04	30 ± 30, 350 ± 70	1.82	No
CaF_2(Eu)	3.19	17	435	0.9	40 ± 30	1.44	No
^{6}LiI(Eu)	3.49	54	470	1.4	—	1.96	Very
BaF_2[e]	4.89	53	310, 220	0.62, 0.0008	—	1.49	No
CsF	4.11	53	390	0.004	—	1.48	Very
$CdWO_4$	7.90	64	480	5.0	—	2.20	No
$GdSiO_5$(Ce)	6.71	59	430	0.06	—	1.85	No

[a]Data from Knoll (1989); *Harshaw Scintillation Phosphors* (1975); Melcher (2000); Derenzo *et al.* (2000).

[b]$Bi_4Ge_3O_{12}$, Lu_2SiO_5(Ce), and $GdSiO_5$(Ce) are often referred to as BGO, LSO, and GSO in the literature.

[c]Data are for room temperature.

[d]CsI(Tl) is better suited to be used with a photodiode because its emission spectrum does not match well with the response spectrum of a photomultiplier tube.

[e]BaF_2 has two dominant peaks in its emission spectrum. When two values appear in this row, the value for the faster scintillating component is given second.

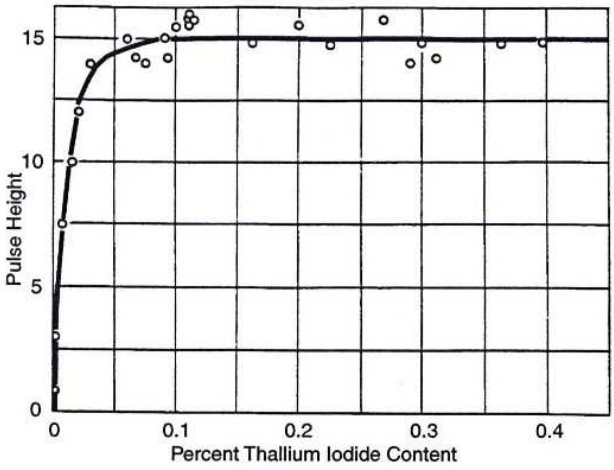

FIGURE 11 Crystal light output as a function of Tl activator concentration in NaI(Tl).

problem of nonuniform distributions of the activator dopant, and good thermal stability in the scintillation characteristics.

The concentration and the distribution of the activator in an extrinsic scintillation crystal affects the light output and detector performance. The activator concentration is important because a threshold amount is necessary to enhance electron mobility and provide uniform light output in the bulk material. Figure 11 shows the activator concentration of thallium in NaI(Tl) as a function of crystal light output (Harshaw *et al.* 1952). The concentration of the activator throughout the scintillator should be as uniform as possible because small localized variations in the light output directly affect the energy resolution of the scintillator.

There are several mechanisms for light output in scintillators; the role of activation centers in an extrinsic scintillator is discussed here. The scintillation mechanism for intrinsic scintillators is described in Rodnyi (1997).

The energy difference observed in the activator band gap of an extrinsic scintillator is related to the wavelength of the photon emitted during the electron transition from the most excited state to the ground state. The maximum energy of the emitted photon can be calculated from the energy-wavelength relationship:

$$E_{\max} = h\nu = \frac{hc}{\lambda_{\max}} \tag{8}$$

where $\lambda_{\max}$ is the maximum wavelength observed in the emission spectrum. Using data for NaI(Tl) taken from Figure 12, a quick calculation yields a maximum single-photon energy of 3.8 eV. As expected, the value is less than the band-gap value of 5.9 eV reported in the literature (Lempicki *et al.*, 1999). The difference between these values is the remaining energy difference between the valence and conduction bands.

Figure 12 shows emission curves that were determined

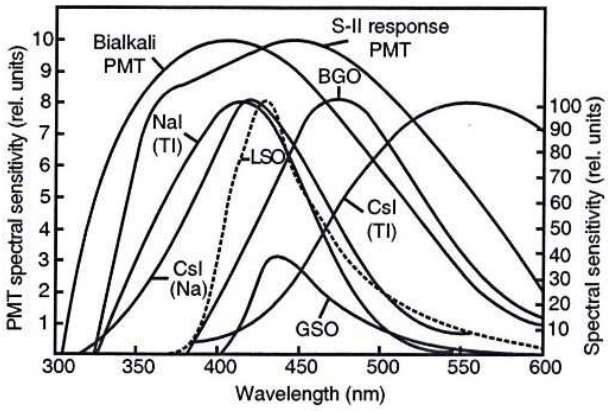

FIGURE 12 Light output intensity for various scintillators and PMT response versus wavelength.

experimentally for several common scintillation detector materials along with the response curves for two different photocathodes. The observed peak emission wavelength represents the most probable transition between the band gaps in the activation center.

It is known that band gaps are discrete quanta; however, we see that the measured emission spectra are smooth curves. The reason for this is that the band-gap structure is in fact more complicated than can be explained by the simple model presented here.

2. Scintillation Conversion Efficiency

We have seen that the electron-hole pairs are created in the crystal as the photon deposits energy into the crystal. Only a certain percentage of incident photon energy is actually converted into electron-hole pairs and, eventually, scintillation light. During the process, some of the energy is lost to X-ray emission, impurity quenching, concentration quenching, and (largely) to internal heat (phonons).

Lempicki *et al.* (1999) express light output L, the number of photons per million electron volts, as:

$$L = \frac{10^6}{2.3E_g}\beta SQ \tag{9}$$

where β is the conversion efficiency in number of electron-hole pairs created per million electron volts of incident ionizing radiation, S is the efficiency with which the electron-hole pairs transfer energy to the luminescence centers, and Q is the luminescence center quantum efficiency in its excited state. All these parameters have been examined here. The term, βSQ is called the *total scintillation efficiency* and sometimes called η. This expression for light output shows that a good scintillator must have (1) efficient creation and trapping of electron-hole pairs, (2) enough electron-hole mobility to allow recombination, and (3) minimal thermal quenching of the excited states.

Because the light output is inversely related to the band gap, we expect the light output to increase continually as

TABLE 3 Additional Properties of the Common Scintillation Detector Crystal Materials[a]

Material[b]	Band-Gap Width (eV)	Total Light Yield (photons/MeV)	Absolute Scintillation Efficiency for Fast Electrons (%)	Output Relative to NaI(Tl) on a Bialkali PMT	Measured Energy Resolution at 662 keV	Calculated PMT Resolution from Photoelectron Yield	Calculated Limiting Resolution at 662 keV
NaI(Tl)	5.9	37,700	11.3	1.00	6.5	3.1	5.7 ± 0.2
$Bi_4Ge_3O_{12}$	5.0	8200	2.1	0.13	9.3	8.1	4.2 ± 0.4
CsI(Na)	6.4	38,500	11.4	1.11	7.4	3.3	6.6 ± 0.3
CsI(Tl)[c]	6.4	64,800	14.9[d]	0.49	7.3	4.3	5.9 ± 0.3
Lu_2SiO_5(Ce)	6	30,000	—	0.75	7.9	4.4	6.6 ± 0.4
CaF_2(Eu)	12.2	23,650	6.7	0.78	—	—	—
^{6}LiI(Eu)	6.1	11,000	2.8	0.23	—	—	—
BaF_2[e]	10.6/18.0	≈9950	4.5	0.13	7-8	6.2	4 ± 1
CsF	9.8	—	—	0.05	—	—	—
$CdWO_4$	—	15,300	3.8	0.18	6.8	5.2	4.4 ± 0.4
$GdSiO_5$(Ce)	—	10,000	—	0.25	7.8	6.2	2.7 ± 1.0

[a]Data from Knoll (1989); *Harshaw Scintillation Phosphors* (1975); Melcher (2000); Lempicki *et al.* (1999); Holl *et al.* (1988); Valentine *et al.* (1993); Dorenbos *et al.* (1975). PMT, photomultiplier tube.

[b]$Bi_4Ge_3O_{12}$, Lu_2SiO_5(Ce), and $GeSiO_5$(Ce) are often referred to as BGO, LSO, and GSO in the literature.

[c]CsI(Tl) is better suited to be used with a photodiode because its emission spectrum does not match well with the response spectrum of a PMT.

[d]Calculated based on total light yield (from Valentine *et al.*, 1993).

[e]BaF_2 has two dominant peaks in its emission spectrum. When two values appear in this row, the value for the faster scintillating component is given second.

the band gap decreases. In reality, we observe that as E_g decreases, Q also decreases because nonradiative transitions dominate the transfer of energy and the scintillator begins to self-absorb its light. Consequently, Eq. (9) is a good first-order approximation of the model, but other higher-order factors are required in this expression to correct for these physical characteristics.

The fractional amount of energy deposited into the crystal that eventually becomes scintillation light is the absolute scintillation efficiency (See Table 3). The measurements reported here were done using a photodiode because it has wide spectral response (Holl *et al.*, 1988; Sakai, 1987). Previously reported measurements were done using a photomultiplier tube (PMT) with an S-11 response curve (see Fig. 12). Notice that there is poor wavelength matching between the PMT response curve and CsI(Tl)'s light output curve.

Robbins (1980) shows that a minimum energy of $\xi_{min} = \beta E_{gap}$ ($\beta = 2.3$) is required to create a single electron-hole pair. Van Eijk (2000) reports $\beta \cong 2$–3 is possible, depending on the crystal material. For NaI, which has a band gap of 5.9 eV (Lempicki *et al.*, 1999), the energy per electron-hole pair is approximately 15.3 eV. By calculation, the maximum number of electron-hole pairs created by a 511-keV gamma-ray absorbed in the crystal is approximately 3.3×10^4. Using the absolute scintillation efficiency of NaI(Tl) given in Table 3 of 11.3%, for the same 511-keV gamma-ray we calculate approximately 1.9×10^4 photons with an average energy of 3 eV. This gives a ratio of 0.57 photons created for every electron-hole pair. This ratio is a measure of the ability of the scintillator to transfer energy to the activation centers, the transfer efficiency. The number calculated here agrees closely with the value of 0.59 derived by Lempicki *et al.* (1999).

3. Thermal Effects on Light Output

As previously discussed, the scintillator luminescent quantum efficiency, Q, is affected by thermal quenching in the excited states of the activation centers. Experimentally it is observed that the light output of a scintillator varies with temperature (Valentine *et al.*, 1993; Kobayashi *et al.*, 1989: Harshaw Radiation Detectors, 1984). Figure 13 shows the measured light output (normalized) of several scintillators as a function of temperature. For each material, notice the temperature at which the light output maximum occurs. Also, note the rate of change of the scintillator's light output around room temperature for each material shown. In some cases, it is possible for a crystal to have a temperature gradient over its volume. As this occurs, the light output throughout the volume of the crystal varies and the energy resolution of the detector will degrade.

4. The Scintillation Light Pulse

Each crystal material emits a well-defined light pulse during the scintillation process. Some scintillator materials have several components to the light emitted. A typical pulse shape is shown in Figure 14. The rise times and decay

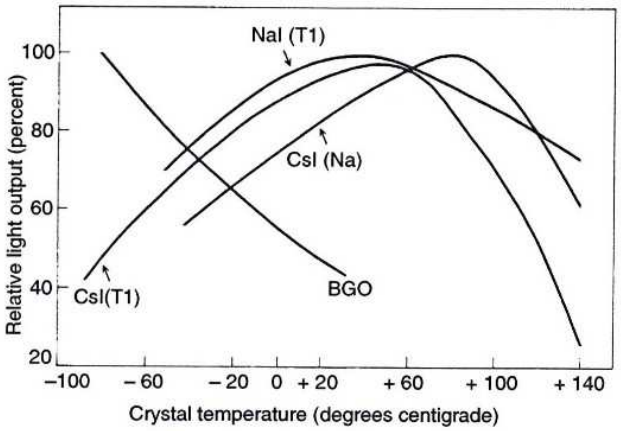

FIGURE 13 Measured light output of several crystal materials as a function of temperature.

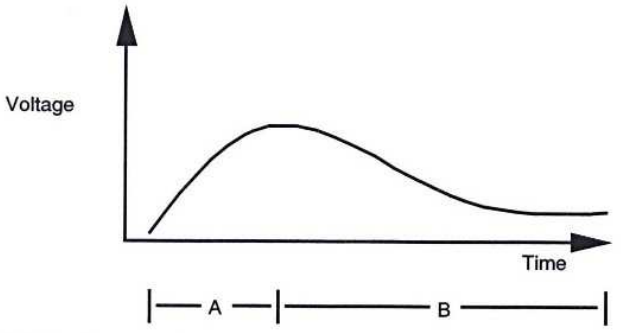

FIGURE 14 Typical scintillation pulse as seen at the PMT anode.

times for each material are well known. Table 2 gives values for the rise time and decay time of the common scintillation materials. Pulse rise times are expressed as the portion of the pulse between 10 and 90% of the total pulse rise time. Pulse decay times are expressed as the amount of time it takes to reach $1/e$ of the total duration of the decay.

The amplitude of the pulse shown in Figure 14 is dependent on several factors:

1. The amount of energy deposited in the crystal.
2. The factors influencing light output in the scintillator.
3. The factors influencing the functional light output of the scintillator.
4. The light collection efficiency of the photodevice coupled to the scintillator.
5. The signal processing capability of the system electronics.

It was stated earlier that in an ideal scintillator the light output would be in the form of a delta function (see Fig. 3). A counting system could then easily discriminate between two slightly different photon energies. Because the photopeak width varies with the parameters given here, obtaining an ideal spectrum is not possible.

Materials that have fast rise times and fast decay times are useful in applications in which high count-rates or timing is important (e.g., positron emission tomography, PET). Narrower pulse widths allow faster data acquisition to occur at higher rates. For example, during PET imaging less imaging time is required, providing some attractive benefits, including better image quality due to less patient motion, less patient discomfort, and more patient throughput.

The rise time of the light pulse follows the familiar exponential dependence:

$$I_A(t) = -I_0 e^{-\lambda_r} \tag{10}$$

where λ_r is the characteristic time that it takes to occupy the activation centers for a given crystal material.

The decay time for all scintillators is greater than the rise time. The decay of the light pulse follows also follows an exponential dependence:

$$I_B(t) = -I_0 e^{-\lambda_d} \tag{11}$$

where λ_d is the characteristic transition probability for the crystal material. The total waveform shape can be approximated by the sum of these two expressions.

Some scintillators have two or more components to the decay time. Ideally, decay time should be short in high-count-rate applications so that electronic pulse pile-up does not occur. Pulse pile-up occurs when two discrete pulses are superposed on top of one another in order to change the shape of the observed pulse. By taking the inverse of the total pulse duration, we obtain an idea of the count-rate limitation for each material. NaI(Tl) is count-rate-limited to approximately 700 kHz, whereas LSO is count-rate-limited at over 2000 kHz.

A closely related concern is scintillator afterglow. Afterglow is a postluminescence in the scintillation material following the removal of a radiation source. Scintillator afterglow results from high concentrations of unwanted defects and impurities in the crystalline lattice. These defects and impurities create luminescence centers in the scintillator, where electrons or holes can be trapped. The light pulse emitted from these anomalous centers typically has a longer decay time. The longer decay time is a problem because it contributes to DC baseline shift and pulse pile-up.

The light output associated with an allowed transition typically occurs within 10^{-8} s after excitation; this type of radiation is referred to as *fluorescence*. After observing the decay times given in Table 2, it is reasonable to inquire why the pulse decay times are reported in microseconds. The explanation is in how the quantum states are formed and what transitions are allowed. The transitions that occur through an impurity or defect site are associated with metastable transitions that are much longer decay times; this type of radiation is called *phosphorescence*.

The decay time of the scintillation pulse is effected by the ambient temperature. Measurements taken (Schweitzer and Ziehl, 1983) show that the decay time for NaI(Tl) decreases by a factor of 4 in the temperature range from

–25°C to +180°C. To further complicate matters, the activator concentration has an effect on the decay time. Eby and Jentscheke (1954) demonstrated the time dependence of the decay with the thallium concentration in NaI(Tl) to vary as much as 50% from the value of 230 ns given in Table 2.

B. Scintillator Energy Resolution

Scintillators are mainly used because of their ability to provide reasonable energy resolution and detection efficiency conveniently and at a reasonable cost. The following section on measurements discusses in more detail how applications are affected by pulse-height resolution (PHR). The previous discussion has shown that the most dominant factor in achieving good PHR is photon yield.

The energy resolution of the detector-PMT apparatus can be written as:

$$R^2 = R_t^2 + R_i^2 + R_n^2 + R_{PM}^2 \qquad (12)$$

Where R_t is the scintillator transfer efficiency, R_i is the measure of the inhomogeneities in the scintillator, R_n is the nonproportional response of the scintillator, and R_{PM} is the photomultiplier tube resolution. As R decreases, the energy resolution improves because the system is then capable of separating gamma rays of different energies. The first three terms in the expression incorporate the contribution of the scintillator and the last includes the contribution of the photomultiplier tube. As each one of these three terms decreases, the energy resolution improves, as expected.

The transfer efficiency term includes the factors that affect how the light that is created in the crystal is converted to electrons in the PMT. Examples of these factors include light transmission in the crystal, nonuniform light collection due to geometric effects, nonuniform surface preparation of the scintillator, nonuniform reflector performance, improper light coupling between the crystal and the PMT, photocathode nonuniformities, poor crystal-PMT wavelength matching, and other PMT response nonuniformities.

The second term in Eq. (12), R_i, is related to the nonuniform distribution of luminescence centers in the crystal. For NaI(Tl), the Tl concentration can vary to contribute to localized variations in light output. Imperfections in the crystal lattice introduced during crystal growth, such as, flock, haze, bubbles, and other point defects, cause variations in the localized light output. Again, these factors degrade the PHR of the detector.

The third term in Eq. (12), R_n, includes the factors that cause the scintillator to respond nonlinearly as a function of energy deposited in the crystal. Numerous studies (Valentine *et al.*, 1993; Kobayashi *et al.*, 1989; Harshaw Radiation Detectors, 1984; Zerby *et al.*, 1961; Narayan and Prescott, 1968; Meggitt, 1970; Dorenbos *et al.*, 1975; Schweitzer and Ziehl, 1983; Eby and Jentschke, 1954; Prescott and Narayan, 1969; Valentine and Rooney, 1994; Fonte *et al.*, 1991; Iredale, 1961; Murray, 1975) report experimental results that have been obtained for NaI(Tl) crystals. By impinging electrons of various energies onto the crystal the light output response function can be determined.

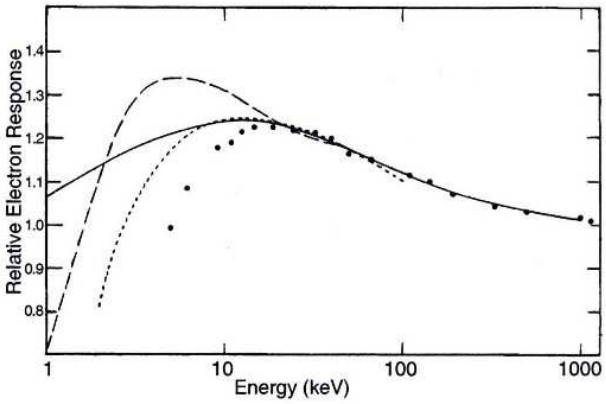

FIGURE 15 Electron response curves.

Prescott and Narayan (1969) present data showing that the measured electron response curve varies as a function of electron energy in NaI(Tl). The curves given in Figure 15 show that there is a nonlinear electron response over the energy range of 1 keV to 1 MeV. There is reasonably good flat response over the range from 10 to 1000 keV. Taking into account the various interaction mechanisms for a 662-keV photon in NaI(Tl), the electron response can vary as much as 50%. The nonlinear response to electrons in NaI(Tl) does degrade the intrinsic energy resolution of the scintillation detector. Dorenbos *et al.* (1975) review the response data from several scintillators including NaI(Tl), CsI(Tl), CsI(Na), BGO, CaF_2(Eu), $CdWO_4$, BaF_2, and LSO(Ce).

The electron response is a measure of mean light yield per unit of electron energy deposited in the crystal. The experimental curves given in Figure 15 show this ratio plotted against energy. This nonproportional or nonlinear response occurs as a result of the statistical process during the creation of secondary electrons. Recall that the incident photon energy with E_γ less than 1.0 MeV transfers energy to the electrons in the crystalline lattice by several possible combinations, including one or more Compton scattering events, a photoelectric event, and X-ray or Auger transitions. In this process a spectrum of electrons of varying energies is obtained. Because the experimental data show us that the total amount of energy absorbed for each incident photon varies, the light yield varies depending on the way in which the photon transfers its energy.

Another contributor to the nonproportional response in the scintillator occurs at the surface of the crystal. Some of the energy may be lost during multiple interaction events due to inefficient transfer or energy loss at the surface of the crystal (Meggitt, 1970).

The last term in Eq. (12), the PMT term, R_{PM}, includes statistical fluctuations due to the number of photoelectrons created at the photocathode. R_{PM} is related to the photon yield N by $1/\sqrt{N}$. It is obvious that as the photon yield increases the system resolution decreases, as expected.

The measured energy resolution for several scintillators is shown in Table 3. The limiting values for each scintillator were determined by Dorenbos *et al.* (1975) as follows:

$$R_{s\ limit} = (R^2_{s\ measured} + R^2_{PM\ calculated})^{1/2} \quad (13)$$

where $R_{PM\ calculated}$ is determined from experimentally determined photoelectron yields while correcting for variations in the PMT gain.

Of the three terms found in Eq. (12), R_t the transfer efficiency, contributes the greatest amount of spread to the photopeak width in NaI(Tl). The nonuniformities mentioned are all dominated by statistical fluctuations during the collection of the photoelectrons. As a result, the gamma-ray energy resolution is approximately inversely proportional to the square root of the photon energy. Statistical fluctuations alone indicate that the PHR for NaI at any energy is a straight line represented by:

$$\ln R_{s\ measured} \cong \ln K - 0.5 \ln E \quad (14)$$

where K ($\cong$ 0.14) is a proportionality factor and E is given in units of mass times the square of the speed of light (m_0c^2). Experimentally determined values for NaI(Tl) obtained by Beattie and Byrne (1972) were shown to be in good agreement with Eq. (14), except that the slope is not as steep as expected because other factors contribute to the widening of the photopeak. These data were gathered in 1972. Today the results follow the same relationship; however, the PHR for NaI(Tl) is much better than that reported by Beattie and Byrne.

C. Material Density

Scintillating materials attenuate gamma-rays by the following expression:

$$I(x) = I_0 e^{-\mu\rho x} \quad (15)$$

This expression is sometimes called the *pencil beam equation*. The initial intensity of a collimated monoenergetic photon beam is reduced by the exponential correction factor, which is dependent on the mass attenuation coefficient (μ), the density of the material (ρ), and the thickness of the material (x). The mass attenuation coefficient is a sum of the interaction mechanisms described earlier in this chapter. The stopping power of the material is greatly increased with small increases in the density or the thickness of the absorber. The effective atomic number, shown in Table 2, is good indicator of a scintillator's stopping power. For photons interacting at photoelectric energies, the effective atomic number is calculated by:

$$Z_{eff} = \left(\frac{\sum_i w_i A_i Z_i^4}{\sum_i w_i A_i} \right)^{1/4} \quad (16)$$

where w_i is the weighting factor, A_i is the atomic mass, Z_i is the atomic number, and the summations are over all of the molecular constituents.

The 1D expression given in Eq. (15) is useful for determining a first-order approximation of detector efficiency. Integrating over the all the potential photon path lengths and assuming equal weighting provides a more accurate result. The most accurate prediction involves a method of calculation called a *Monte Carlo simulation* (see Chapter 25 in this book).

Recall from the earlier discussion that the gamma-ray interaction probability is strongly dependent on both the electron density of the crystalline structure and the atomic number of the nucleus. The greater the number density of the electrons in the crystalline lattice, the more likely it is that the impinging photon will be attenuated by Compton scattering. The greater the atomic number, the greater the probability that a photon will be absorbed in the photoelectric process. The densities and the effective Z of several materials are given in Table 2.

The plot given in Figure 16 shows the attenuation curves for the 140 keV gamma ray of Tc-99^m and the 511 keV gamma ray of Na-22 in NaI(Tl) and BGO. These results were obtained using the pencil beam expression. A SPECT (single-photon emission computed tomography) gamma camera's typical thickness is 9.5 mm. The plot shows that 90% of the 140-keV photons of Tc-99^m are attenuated in the NaI(Tl) crystal. A PET imaging device with a 19-mm-thick NaI(Tl) crystal attenuates 45% of the 511-keV gammas, whereas the same thickness of BGO attenuates 85% of the 511-keV photons.

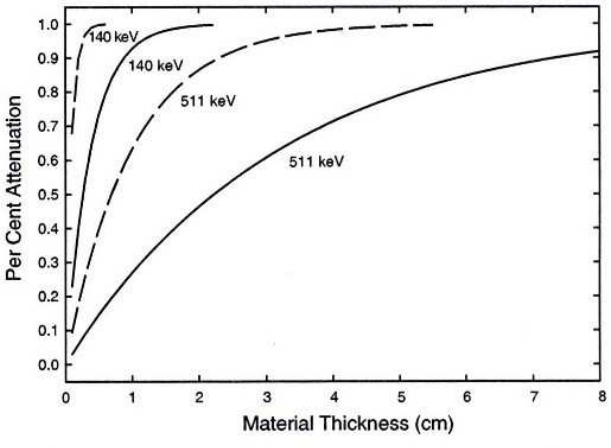

FIGURE 16 Attenuation curves for the 140 keV gamma ray of Tc-99m and the 511 keV gamma ray of Na-22 in NaI(Tl) (solid line) and BGO (dashed line).

A more detailed calculation takes into account the fact that the detector housing, or energy entrance window, reduces the number of photons available for detection according to the density and mass attenuation coefficient of the housing material. Typically, scintillator housings are built with thin-walled aluminum, so that the signal from the source is not reduced significantly. Aluminum is a low-Z material ($Z = 13$); however, for very low energy gamma-counting applications in the range of 5 to 30 keV, counting efficiency is increased substantially by using a thin piece of beryllium ($Z = 4$) as the energy entrance window.

D. Optical Properties

Several optical properties influence the performance of scintillators. The discussion here refers to the optical properties of light transmission, light absorption, and light reflection.

In order to optimize the performance of the scintillator, it is important that nearly all the light that is created in the scintillator is detected at the photocathode of the PMT. The light that is created in the scintillator must not be self-absorbed by the crystal; that is, the crystal must be transparent to its own light. As previously stated, good scintillators have emission band gaps that do not overlap with the optical absorption band gaps because an overlap causes excessive self-absorption of light in the crystal. Self-absorption can occur due to unwanted impurities quenching the light output of the scintillator. These impurities may be present in the original growth material or they may be introduced into the crystal during growth. Typically, elemental impurities are controlled to part-per-million concentrations.

Visual inspections for optical clarity often give a good indication of the quality of the crystal material. Materials that transmit in the visible regions of the spectrum and are water white in general perform quite well. Some scintillation materials such as LiI and ZnS must be used in thin sections because they have significant self-absorption.

Additional light losses can occur because the scintillation light reflects on the inside surface of the crystal. During the manufacturing process these crystal surfaces are prepared to minimize light loss at the surface and enhance uniform collection at the photocathode.

It is interesting to note that the optical properties of scintillators typically do not depend on the lattice orientation. Only in the case in which significant impurities have built up around domain boundaries does this become an issue. In particular, the image quality in gamma-camera plates is sometimes degraded when the light output across a grain boundary is affected.

The light available to enter the photocathode is influenced by the index of refraction of the material. The index of refraction (n) of air is close to unity, the index of glass is typically between 1.5 and 1.7, and the index of fused quartz is approximately 1.47. The index of refraction for most scintillation materials is between 1.44 and 2.20 (see Table 2). Remember that, if the index of refraction does not match well, then one component of the light is reflected and one component is refracted at the interface. This can either be beneficial or detrimental to the process of maximizing the light collected at the photocathode.

Total internal reflection of the light occurs in a material at the critical angle or Brewster's angle, which is given by:

$$\theta_c = \sin^{-1}(n_2/n_1) \tag{17}$$

where n_1 is the index of refraction of the material in which the light originates, and n_2 is the index for the material across the interface. That is, if the angle of incidence, as measured from the normal, is greater than θ_c, then all light incident at these angles remain in the crystal. NaI(Tl) has a critical angle of 32.7°, whereas BGO has a critical angle of 27.7°. Less light escapes a crystal with a higher index of refraction, unless some design feature is used to improve the light coupling to the PMT.

For angles of incidence less than the critical angle, it is important that a good diffuse reflector is used to return the light into the crystal. Reflectors that are used typically have coefficients of reflectivity greater than 0.95 at the wavelengths of concern. Some of the common materials used are Teflon, Al_2O_3, MgO, and high-reflectance papers. In the construction of scintillation detectors, the interface is actually crystal-air-reflector. Noting this is important. If the material adjacent the crystal has an index near that of the crystal material, then the light will more easily be coupled away from the crystal and some percentage of it lost due to the use of imperfect reflector materials.

At the optical interface to the PMT, ideally all incident light should pass directly through to the photocathode. Thin films of a silicon elastomer ($n \cong 1.43$) are used most often to glue the crystal to the PMT. These interface materials efficiently couple the light from the crystal to the PMT and they are selected because of good transparency at the appropriate wave length and good refractive-index match.

E. Mechanical Properties and Intrinsic Background

The mechanical properties of scintillation crystals have been characterized and reported (*Harshaw Radiation Detectors*, 1984; NASA, 1973, 1974, 1980; Ishii and Kobayashi, 1991). Some useful mechanical properties are given in Table 4.

Some crystal materials have unavoidable intrinsic background. A good example of this is the material LSO. The isotope of ^{176}Lu in LSO has a natural abundance of 2.6%, and has gamma-ray energies at 89, 202 and 307 keV. These photons contribute approximately 300 cts/s-cc of LSO material. In PET applications, the energy of interest is around 511 keV, so the background signal in LSO is not a problem.

TABLE 4 Useful Mechanical Properties of the Some of the Common Scintillation Detector Crystal Materials[1]

Material	Hardness (Mohs)	Cleavage Plane	Thermal Coefficient of Linear Expansion (%/°C × 10^{-6})	Melting Point (°C)	Radiation Hardness (rad)	Machinablitiy
NaI(Tl)	2	100	47.4	651	10^3	Carbide tools on standard lathes and mills
$Bi_4Ge_3O_{12}$	5	None	7	1050	10^{4-5}	Diamond tools at high speed
CsI(Tl)	2	None	54	621	10^3	Carbide tools on standard lathes and mills
CsI(Na)	2	None	54	621	—	Carbide tools on standard lathes and mills
CaF_2(Eu)	4	111	19.5	1418	—	Diamond tools at high speed
BaF_2	3	111	18.4	1354	10^{6-7}	Carbide tools on standard lathes and mills
LiI(Eu)	2	100	40	446	—	Carbide tools on standard lathes and mills
CsF	2	100	31.7	682	$<10^4$	Carbide tools on standard lathes and mills
$CdWO_4$	4–4.5	010	10.2	1325	10^3	Diamond tools at high speed
LSO	5.8	None	—	2070	10^{6-7}	Diamond tools at high speed

[1]Harshaw Radiation Detectors (1984); NASA 1973, 1974, and 1980; Kobayashi *et al.*, 1993.

Standard NaI(Tl) crystals, with less than 1 ppm potassium, exhibit some background due to a background contribution from ^{40}K. ^{40}K has a natural isotopic abundance of 0.01% and E_γ = 1461 keV with a branching ratio of 11% and $E_{\beta-}$ end-point energy of 1314 keV and a branching ratio of 89%. An activity calculation yields approximately 0.02 ^{40}K events/min/cc in NaI(Tl). When placed in a lead safe for several hours, a very large-volume crystal (≅ 4000 cc) made from standard material exhibits a ^{40}K gamma spectrum. To reduce the amount of ^{40}K present in a crystal used in very low-background-counting applications, the crystal material can be grown twice. Assemblies that are carefully constructed with low-background materials can achieve count rates as low as 5 cps in the energy window of 200–3000 keV.

BGO can also have a background count rate as high as 7 events/s/cc if great care is not taken to ensure that the starting growth material is not contaminated with ^{206}Pb. Cosmic protons that transmute ^{206}Pb to ^{207}Bi, which has a $T_{1/2}$ = 38 years, will contribute gamma background at energies of E_γ = 570, 1060, 1630 (sum), and 2400 keV. If the starting material is obtained from lead-free ores, this contamination is not present.

IV. SCINTILLATION DETECTORS: DESIGN AND FABRICATION

The optimal design of any scintillation detector depends on a good understanding of physical properties and characteristics and their relation to scintillator performance. It is likely that several design iterations will occur on paper before a final design is found. The final detector design invariably is a compromise of the ideal design. This section discusses various design issues and then describes how a scintillation detector is manufactured.

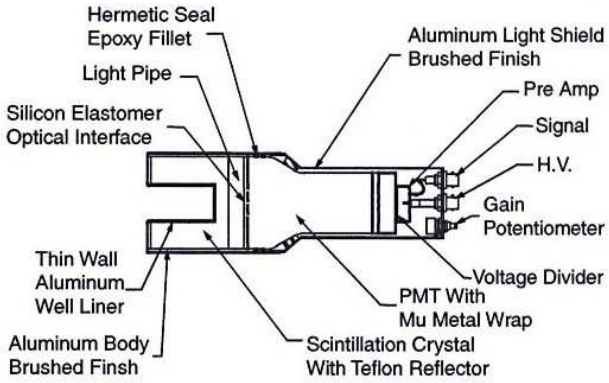

FIGURE 17 Scintillation detector diagram.

A. Detector Design

Figure 17 shows an integral-type well detector, which has the PMT mounted integrally to the crystal. Figure 17 shows all the other major detector components, including the reflector, silicon elastomer optical interface, hermetic seal, light shield, voltage divider, preamp, high-voltage input, and signal output. Well detectors are used in applications in which an increased solid angle is important to increase counting efficiency. Two common applications for well detectors are environmental sample counting and radioimmunoassay sample preparations.

The previous section explained in detail the importance of the light output of the scintillator. Because most scintilla-

tor applications involve spectroscopy, the most important design criterion is the energy resolution of the detector. Each experiment or application has its own set of design issues; the following provides a good starting point:

1. *At what energy is the gamma ray of interest? What is the anticipated signal strength (activity) of the sample to be measured?* The mass attenuation curves are a useful tool because we can determine an optimal thickness for the scintillator. To ensure that reasonable counting times are obtained, the geometry must be selected to achieve good counting efficiency. At the same time, too much material may cause unwanted background to be introduced into the spectrum and reduce the signal-to-noise ratio (SNR). If the gamma-ray energy is less than 100 keV, then the count rates and the total counting times will be improved if a low-Z material, such as a thin piece of beryllium, is used as the energy entrance window. At higher energies, gammas have a higher penetration probability, so there is much less signal lost to absorption in the crystal housing.
2. *Are there multiple gammas in the sample? If so, what PHR is required to separate the peaks?* These questions are important because the energy resolution must be good enough to separate the photopeaks at a reasonable confidence level. The design may require the selection of premium crystal material during the manufacturing process to ensure that adequate PHR is achieved. The best NaI(Tl) detectors that are produced will achieve slightly better than 6.5% at 662 keV. The selection of premium material will add cost to the detector. A good rule is to maintain a geometric aspect ratio of 1:1 to obtain the best energy resolution.
3. *Is there significant gamma background that will degrade the signal-to-noise ratio?* If significant background is present, the designer should consider shielding the detector or collimating the signal to improve the SNR. In some multiple-detector configurations, tungsten septa are placed between the individual elements to reduce cross-talk from Compton scattering. At the same time, the crystal geometry should be carefully selected. It should be optimized to the gamma energy of interest and to account for any directionality of the source.
4. *Where will the detector be used?* If the detector is used in laboratory conditions, the design requirements are much less stringent than if the detector is going to be incorporated into a space mission. Typically, detectors are manufactured to meet a certain level of shock and vibration specifications because the assembly must withstand handling during the shipping process. All designs must meet minimum mechanical and thermal-shock protection specifications, and they are warranted to meet these specifications. Other environmental conditions that affect the design are humidity and pressure.
5. *Is detector compactness important?* Some applications minimize the amount of material between multiple detector segments because the scientist is concerned about the loss of good signal. Introducing unwanted background through gaps in shield detectors can also be a concern. If compactness is a significant issue, the denser scintillation materials should be considered. The first PET imaging systems were built using NaI(Tl) crystals. Eventually, BGO and LSO became popular because they improved the overall performance due to their higher density. The higher density means more detector elements per solid angle subtended, better stopping power, and improved spatial resolution. An added benefit is that BGO and LSO are nonhygroscopic, which removes some significant engineering problems associated with providing a good hermetic seal.
6. *Should the PMT be demountable?* Some uses require that the crystal be demountable from the PMT assembly. This is useful when it is anticipated that damage can occur to either the crystal or the PMT; then only one component has to be repaired. This is especially true for detectors that are used in the field. When the assembly is designed with a demountable PMT, the PHR will degrade slightly due to the additional interface material and glass between the crystal and PMT photocathode.
7. *Will the application require multiple detectors?* At some point, the designer must consider the trade-offs between a large detector, multiple detectors, or detectors with multiple elements. The size of any detector is limited by the capabilities of the crystal-growth manufacturer. As expected, a larger crystal element increases the cost of the crystal. Some of the large crystal cost, which might have only one PMT, is offset by the cost savings associated with the cost of gain-matching the elements, the cost of the electronics to process the signal from multiple PMTs, or the cost of multiple detectors. Assembly costs also contribute to determining the best approach to minimize the cost of the detection system. Some detectors can require multiple, optically isolated elements to achieve the intended use.
8. *Is the scintillator pulse shape important to the application?* Some applications use the fast rise time as a technique for counting events. These applications, which are referred to as timing measurements, depend on fast electronics to obtain good data. Applications with high count rates can be concerned with the amount of afterglow present in a scintillator because afterglow can cause pulse pile-up. Afterglow lengthens the decay time due to impurities in the crystal material. At high count rates, the lengthened pulse shapes overlap and lead to pulse pile-up.
9. Finally, economics must be considered. Each design decision has a cost impact and a cost-benefit analysis should be done to determine the usefulness of all of the design options.

These design questions are typically reviewed by the manufacturer and customer before a project is initiated.

B. Detector Components

Each component that goes into a scintillation detector has numerous properties that can affect the overall performance of the detector. These component issues are continually being investigated to improve the quality of the product.

1. Crystal

Previous discussion has dealt with the many parameters important to obtaining the best performance crystal material can provide. To achieve the highest quality scintillation material, the starting material used to grow an ingot must be the highest purity available. Crystal growers along with material scientists are continually looking for ways to improve the quality of the scintillator by removing impurities from the starting material. The techniques used to grow the crystal ingots are also improved on with research and experience. Each material has quality issues that are affected by the growth process. Extrinsic scintillation materials must limit the activator or dopant nonuniformities. Gradients in the activator distribution cause nonuniform light output and the performance of the detector is degraded.

2. Reflector

A good reflector has high reflectivity at those wavelengths in which the scintillator emits light. It has the ability to form itself closely to the surface of the crystal. However, the reflector should not wet the surface because this will pipe light away from the crystal. Historically, MgO, Al_2O_3, and TiO_2 were used as reflector materials. Powders are difficult to dry, are messy, and do not have the best reflectance. Powders have been replaced with Teflon, which is hygrophobic, easy to form around the crystal, and not messy. Other paper reflectors are used in applications in which the Teflon is not stiff enough to hold its form.

3. Interface Materials

The best interface materials have the following properties: good light transmission at the wavelengths of interest, good index of refraction match to the crystal, good adhesive and cohesive strength, good function over a large temperature range, good electrical characteristics, a reasonable coefficient of thermal expansion, easy handling during assembly, and low cost. Both hard interfaces and soft interfaces are used, depending on the application. The hard interface materials are two-part epoxies, and the soft interface materials are two-part silicon elastomers. Applications in which the detector will experience a wide range of temperatures require that the interface, usually a silicon elastomer, be under constant pressure. A crystal grows and shrinks at greater rates than stainless steel because it has a much greater coefficient of thermal expansion. Partial interface separation, causing light loss, does not occur when the detector packaging keeps the interface under pressure.

4. Light Pipes

A glass or quartz window is sometimes placed between the crystal and PMT to improve PHR performance by reducing the nonuniform light response from the crystal or nonuniform response in the photocathode. In counting applications characterized by low count rate and low gamma-ray energy, a light pipe is sometimes used to shield a thin (≈1/16-in-thick) crystal from the K-40 background that is present in some PMT glass. Light pipes can vary in thickness from 0.5 to 2 in thick. Quartz is more expensive to use than Pyrex or borosilicate glass, but it has better light transmission characteristics.

5. Crystal Housing

Crystal housings are usually made out of metals such as aluminum or stainless steel. Aluminum alloys are more machinable and are less expensive than stainless steel. Cylindrical crystal housings are usually spun or formed out of aluminum; however, stainless steel can also be spun. Stainless steel has the advantage that it is more rugged. In some low-background counting applications, it is used because it has less radioactive contaminants than aluminum. In ultralow-background counting applications, oxygen-free hydrogenated copper is used because of its extremely low background count rate.

6. Hermetic Seals and Light Seals

All hygroscopic crystal materials (see Table 2) require a reliable seal to keep the crystal from hydrating. Most detector seals use an epoxy filler between the PMT glass and the crystal housing. All-welded assemblies and special glass-to-metal seals are also very reliable hermetic seals in those applications in which the detector can experience severe mechanical shock and vibration.

As always, great care must be taken to minimize any extraneous background due to contaminated components. When the welded-seal technology was first introduced, it was determined that welding rods contaminated thorium introduced unwanted background into the spectrum. Today, tungsten inert gas welding is used.

Light seals also have an important role in a good detector assembly. If small amounts of ambient light leak to the photocathode, extraneous noise is introduced into the signal and damage may occur to the PMT.

7. Photomultiplier Selection

PMT characteristics that must be considered during the selection process include energy resolution (quantum efficiency), linearity, long- and short-term stability, electronic noise level, gain, photocathode uniformity, photocathode wavelength sensitivity, and PMT rise time. Manufacturers' handbooks and catalogs are very useful in making these selections.

Referring to Figure 17, observe that the PMT is wrapped with a special mu-metal foil. This foil significantly reduces the effect of external magnetic fields on the PMT's performance. If the PMT is stationary, motors, cathode ray tubes (CRTs) and other sources of magnetic fields can affect the PMT. If the PMT is in motion during counting, the Earth's weak magnetic field can affect the trajectory of the electrons from the photocathode to the first dynode.

The best PHR performance is achieved when the photocathode covers all the light exit face of the crystal. PMT photocathodes are usually circular in shape and fit well within a right cylinder.

8. Voltage Divider and Preamp

The PMT manufacturer's recommendations should be followed to obtain the best results. In some cases, the voltage-divider design should be modified for unusual count rates. With normal count rates, a lower-impedance ($\approx$ 5 MΩ) divider string is recommended. If a low count rate is expected and the power supply is current-limited, a high-impedance ($\approx$ 100 MΩ) divider string is recommended. The preamp is used to preserve the signal coming from the PMT anode and output the signal to a linear amplifier.

C. Detector Fabrication

Equally important as the design issues and component performance issues just discussed are the assembly practices and techniques used during the production of a detector. There are several techniques used to grow scintillation materials. The most commonly used growth techniques include Stockbarger-Bridgeman, Czochralski, horizontal Bridgman, radiofrequency (RF) induction, and *in situ* gradient freeze. Some growth techniques make use of growth from the melt; other techniques are from seeded growth; and others initiate nucleation spontaneously. All techniques involve loading salt into a crucible, melting the salt in an electric furnace, and then freezing the material at rates between 1 and 10 mm/h. After the charge is completely grown, it must be slowly ramped to room temperature to avoid thermal shock to the ingot. This process is called annealing the ingot.

Three important factors must be controlled to obtain the highest quality crystal ingots: (1) use the highest purity grade starting material; (2) use the best available growth equipment; and (3) the growth process must be continually monitored with computerized controls.

The assembly of the detector starts by sawing a crystal blank from the ingot. The crystal blank is then machined into the required shape with conventional milling or lathing machinery. Hard oxide crystals, such as BGO, $CaF_2(Eu)$, and $CdWO_4$, require high-speed machinery with special cutters. After machining, the crystal is ready for its final surface preparation. Because some crystal materials are hygroscopic, they must be handled in humidity-controlled environments (refer to Table 2). Special dry rooms are used in the fabrication of NaI(Tl) detectors. A NaI(Tl) dry room operates at very low humidity levels, typically at dew points of –25 to –50°C. Operating under these conditions avoids the performance-degrading formation of hydration on the surface of the crystal.

After the hygroscopic crystal is machined, it is moved into the dry room to let the surface dehydrate. A hygroscopic crystal will have a thin layer of hydrate on its surface, and this opaque white powder can easily be removed with an anhydrous solvent and a mild abrasive cloth such as steel wool. Once the hydrate layer has been removed, an optically transparent surface is visible.

All water of hydration must be removed from the surface so that no light is lost as it reflects off the inner surface of the crystal. Any hydration at the surface will cause a loss of light because the hydrate is a poor reflector. Ideally, all the light should be internally reflected at these inside crystal surfaces and then eventually collected at the interface to the PMT because this gives the best energy resolution.

The cleaned surface of the crystal is then prepared by polishing or abrading the surface to optimize the light output of the crystal. This optimization process, called *compensating the crystal*, improves the PHR by making the light output response as uniform as possible along the length of the crystal. Technicians use a method called *mapping* to determine how uniform the response is for a given compensation. This technique is used frequently when the aspect ratio (length:width) is greater than 3:1. A uniform PHR to within 3% along the length of the crystal gives a good side on energy resolution. At the same time, end-on resolution provides a good indication of the material performance.

The face that is to be coupled to the PMT is polished. In general, all of the surface preparations are done manually due to the fragile mechanical characteristics of the crystal. During these manual operations, the technician must handle the crystal carefully so that the crystal will not fracture by mechanical or thermal shock. A hard oxide crystal may have all of its sides chemically etched, except for a polished face that is coupled to a PMT; sometimes a hard oxide may be polished all over.

At this point in the assembly process, the crystal is ready to be interfaced to a piece of glass or a PMT. The silicon elastomer material acts as an adhesive between the crystal and the glass surface. Elastomers have good mechanical properties because they allow some material movement in shear mode without cohesive or adhesive separation.

The crystal surface is then surrounded with a highly reflective material such as Teflon. The reflector must stay in good contact with the surface of the crystal to avoid light loss at the crystal-reflector boundary. Ideally, the best performance occurs if no light is lost at the surface of the crystal.

Finally the crystal is encapsulated in a metal container such as aluminum or stainless steel by creating a hermetic seal with an epoxy joint between the glass and the metal can. Figure 17 shows a typical detector assembly. Note, again, that it is important that the detector be constructed in such a way that no outside light interferes with the low light signals being generated in the crystal. Once the assembly is completed, it is tested to ensure that all the specifications have been met.

V. MEASUREMENTS WITH SCINTILLATORS

Previously in this chapter the various properties and characteristics of scintillation detectors (absorption of the incident photons, light output, thermal effects on light output, and scintillator energy resolution) have been discussed from a theoretical perspective. In this section, the discussion is related to the practical use of scintillation detectors. The reader can find additional useful information provided by Birks (1964), Knoll (1989), Hendee (1984), Sorenson and Phelps (1987), Hofstader (1975), and Heath *et al.* (1979).

A. Measurement Systems

1. Basic Spectroscopy Counting Systems

A simple gamma-ray counting system is shown in Figure 18. The block diagram includes all the essential components required to obtain a gamma-ray spectrum. The components that make up the signal-processing apparatus are discussed in this section.

a. Detector Assembly—Crystal/PMT/Voltage Divider

The detector assembly consists of the components shown in Figure 17 (see previous discussion). The PMT is required to convert the very low-level light created in the crystal to a signal that is conveniently processed. As the light enters the PMT, it is converted into an electron cloud at the photocathode. These electrons are directed to the first dynode of the PMT by an electric field that is produced by a voltage-potential difference between the photocathode and the first dynode of the PMT. By the appropriate distribution of the voltage between the dynodes in a PMT, (PMTs may have up to 10 dynodes), electrons are focused and multiplied such that a usable analog pulse is generated at the anode (see Fig. 14). The signal that is generated by the crystal/PMT/voltage divider at the anode is a negative-going pulse with amplitude around 50 mV. Typically, these assemblies have high impedance and low capacitance. Some portable low-count-rate assemblies have very high-impedance voltage dividers.

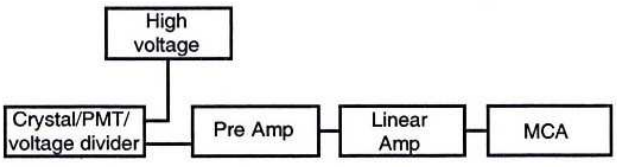

FIGURE 18 Gamma-ray counting system block diagram.

b. High-Voltage Input

High-voltage power supplies are designed to provide up to 2000 V DC with up to 2 mA if required. Most detection systems operate at positive high voltage. Good power supplies are designed to limit noise, limit drift, and hold these specifications over a wide temperature range. The high-impedance voltage divider used in low-current applications (low count rate) use a high-voltage power supply that can be operated with D-cell batteries. This is especially useful in counting systems that are hand-held field instruments.

c. Preamp

Preamps are low-noise electronic devices used to take the input and, without shaping the pulse input, preserve the pulse with the maximum SNR. In most cases, a counting system works quite well without a preamp. The use of a preamp circumvents problems that can occur when different length cables are introduced between the detector and linear amplifier. Changing cables affects the resistor-capacitor (RC) time constant, and this could mean that the linear-amplifier shaping time constants have to be adjusted. The RC differentiation that occurs in the preamp has a relatively long time constant to prevent pulse pile-up. There are three types of preamps: voltage-sensitive, charge-sensitive, and current-sensitive. Spectroscopy applications use a current-sensitive preamp in which the signal is taken from the anode of a PMT. The preamp is capable of taking the signal and driving several feet of cable so that the pulse can be accepted by a fast linear amplifier with minimum distortion. Preamps are designed to provide impedance matching between the detector assembly, cable, and linear amplifier.

d. Linear Amplifier

Signals from the preamp are amplified, filtered, and shaped in the linear amplifier. The linear amplifier takes a nominal 50 mV input and amplifies it to several volts, making the signal suitable for processing in a multichannel analyzer. Shaping and filtering the signal in the amplifier improves the SNR and the response time required for each pulse is reduced. Amplifiers are provided with coarse- and fine-gain adjustments, so that the signal output can be adjusted to a useful voltage. Shaping-time and integration-time adjustments help optimize the signal processing. The time-constant adjustments should be selected to match the pulse shape of the scintillator being used.

e. Multichannel Analyzer

A multichannel analyzer (MCA) is used to obtain the PHR of a scintillator. In an MCA, the analog signal output from the amplifier is digitized and displayed in the form of a histogram. This histogram represents an energy distribution for the events that occurred in the scintillator. MCAs have an adjustable low-level discriminator so that extraneous low voltage pulses will not cause significant counting dead time.

The counting system can be calibrated with an electronic pulser with a known voltage output or by using several radioactive sources to develop an energy-per-channel calibration factor. Because of the slight nonlinearity of the response of scintillation materials, the sources method should be used with caution.

Oscilloscopes are often used to analyze the waveform output form each component in a counting system to ensure that it is operating properly.

With this overview of the basic measurement system, the response characteristics of a basic counting system can now be discussed in more detail.

2. Measurement System Response

The properties of the scintillation crystal have the primary influence on the overall performance of the detection system. It is important that each performance characteristic is understood to ensure optimal system performance. The following discussion addresses the most important system response features.

a. Spectral Response Curve

Section III of this chapter explains that the amount of energy deposited in the crystal is equal to the incident photon energy and that the light output of the scintillator is nearly proportional to the energy deposited in the crystal. This is an essential aspect of detector technology. This feature gives us the opportunity to perform gamma ray spectroscopy. Now, gamma rays of different energies can be recorded and analyzed by energy and by activity.

A gamma-ray spectrum is shown in Figure 19. The spectrum represents a histogram of all the energies recorded by the counting system between 5 and 1000 keV. The histogram records the voltage pulse-height data for each pulse generated by the counting system. Each data point is stored in a bin or channel; each channel has a discrete voltage width. For scintillation counting applications, an MCA typically accepts voltage input from 0 to 10 V; the channel numbers (horizontal display) scale with the binary numbers 256, 512, or 1024. The vertical display scale can be adjusted from the log scale up to over 10^6.

The spectrum shown in Figure 19 is for ^{137}Cs. ^{137}Cs decays to ^{137}Ba by beta decay (β^-). ^{137m}Ba, with a half-life of 3 min, has a monoenergetic gamma-ray at 662 keV. Most studies state that the 662-keV gamma-ray is from ^{137}Cs, and

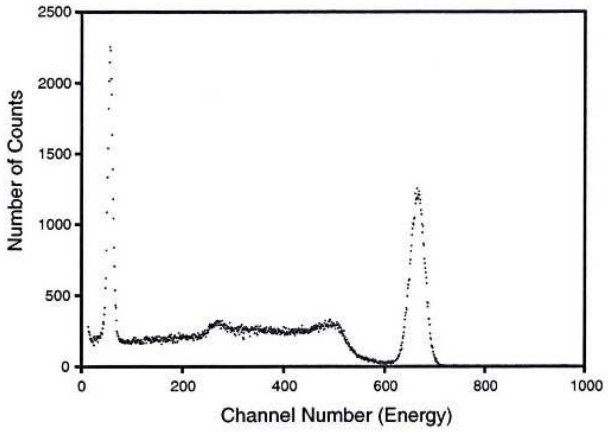

FIGURE 19 Pulse-height spectrum of 662-keV gamma ray of Cs-137.

we do the same here. The main features in the spectrum are the Ba X-rays around 30 keV (CH 35), the backscatter peak around 260 keV (CH 260), the Compton shoulder around 500 keV (CH 500), and the full-energy photopeak at 662 keV (CH664). Other interesting features include the tail of some electronic noise seen around 5 keV and the small number of counts seen in the valley around channel 600. The low-energy electronic noise, which is attributed to the PMT, sometimes limits the low-energy measurement capability of a counting system.

Table 5 shows the expected spectral response for various gamma-ray events in a scintillation detector. A gamma-ray spectrum has a number of predictable features that are summarized here. It is useful to know that the spectral features can be predicted because computer algorithms can be used to look for these response features. Monte Carlo codes are sometimes used to predict the behavior of a counting system.

b. Energy Resolution

Previous sections have discussed how light is produced in a scintillation crystal and the importance of efficient light collection. The ability of the crystal material to produce light and the ability of the detector assembly to collect the light and convert it to a usable signal are the two most important functions of the gamma-ray spectrometer. Each has a direct effect on the energy resolution of the counting system.

The energy resolution or PHR of a detector is defined as the ratio of the full width at half maximum (FWHM) of the photopeak to the mean of the photopeak. A typical PHR for NaI(Tl) is approximately 7.5% at 662 keV. Arithmetically, the PHR (in percent) is written as:

$$\text{PHR} = \frac{\text{FWHM(channels)}}{\text{Photopeak(channel number)}} \times 100\% \qquad (18)$$

For example, examine Figure 19, which shows a gamma-ray spectrum for Cs-137 taken by a NaI(Tl) crystal detector

TABLE 5 Detector Spectral Responses

Interaction Event	Explanation and Observed Spectral Response
Photoelectric	Well-defined peak at E_γ
Compton scatter	A continuum of energies between $0 \leq h\nu' \leq h\nu'_{max}$ according to Eq. (2)
Photopeak/Compton valley	Region of the spectrum between the photopeak and the Compton shoulder that contains multiple Compton scattering events
Pair production (pp)	Peaks observed at 511 keV due to β^+ annihilation events that occur outside of the detector
Backscatter	Peak around 200 to 250 keV due to Compton scattering events that have occurred in materials surrounding the detector
X-ray peak	Peak associated with the emission of a characteristic X-ray from materials that surround the detector
Lead X-ray peak	Peak associated with the emission of a characteristic lead X-ray from lead material that may surround the detector, peak at 80–90 keV
Escape (I-single)	Peak associated with the creation of the K edge X-ray of iodine by photoelectric absorption interaction with I near the surface of the NaI(Tl), the 30 keV X-ray escapes from the crystal and a peak is observed at $E_\gamma - 30$ keV
Escape (pp-single)	Peak observed at $E_\gamma - 511$ keV; E_γ must be $> 2 \times 511$ keV
Escape (pp-single)	Peak observed at $E_\gamma - (2 \times 511$ keV); E_γ must be $> 2 \times 511$ keV
Sum	Peak associated with the coincident detection of two or more photons from simultaneous nuclear transitions
Background	Peaks associated with the presence of naturally occurring K, U and Th in the immediate area
Background	A continuum spectrum due to Compton scatter of naturally occurring background

assembly. This detector has a PHR of 6% at 662 keV. In other words, the photopeak at half maximum is 40 keV wide. The PHR is exceptionally good because it has high-grade NaI(Tl) crystal material and the light collection efficiency has been optimized by a favorable geometry. Most scintillation detectors are manufactured to a PHR specification quoted by the manufacturer.

Three major effects contribute to the width of the photopeak. First, the statistical nature of the photon production, collection, and multiplication of the electrons in the dynode string causes degradation in the photopeak width. Second, each scintillation pulse created has associated with it noise from dark current created at the photocathode. This electronic noise or electronic jitter degrades the width of the photopeak. Third, degradation in the photopeak width is caused by light collection. These variations in the pulse height are due to the nonuniform collection of the light created inside the crystal in spite of careful surface preparation of the crystal to minimize this problem.

Another minor contributor to the line-width spread is the previously discussed nonlinear response of the scintillation material as a function of energy deposited in the crystal (Zerby *et al.*, 1961). Temperature gradients in the bulk material and the temperature at which the measurement are performed also affect the PHR (see the previous discussion on scintillator energy resolution).

c. Peak-to-Valley Ratios

Another parameter that can be used to quantify the quality of a detector is the peak-to-valley ratio. This is simply the ratio of the number of photopeak events in the peak channel to the number of events recorded in a valley channel. For a large-volume detector (5000 cc), the peak-to-valley ratio for ^{60}Co, which has photon energies of 1170 keV and 1331 keV, can be approximately 7:1; whereas a smaller-volume detector (350 cc) can have a ^{60}Co peak-to-valley ratio of approximately 10:1. The detector used in obtaining the spectrum shown in Figure 19 has a ^{137}Cs peak-to-valley ratio of 70:1. The number of photopeak events measured is strongly dependent on the volume of the crystal, whereas the number counts recorded in the valley is strongly dependent on the PHR of the detector. The peak-to-valley ratio specification gives a direct measure of the ability of the detector to measure the separation of two peaks that have energies that are very close to one another.

d. Detector Counting Efficiency

Several factors determine the counting efficiency of a detection system. The factors include the energy of the incident photons, intrinsic efficiency of the scintillation material, geometry of the crystal, losses due to scatter or absorption in the source (e.g., a patient), and losses due to the scattering or absorption of the photons before they reach the crystal due to the finite thickness of the detector housing and other detector assembly components. As previously discussed, the intrinsic efficiency is sometimes related to the temperature at which the detector is operated.

The counting system electronics can also affect the counting efficiency. The electronic apparatus needs a finite time to record each pulse. If additional pulses arrive while

the system is already processing a pulse, then they either pile on top of one another or the pulse is lost because the input gate is closed. In either case, a counting error occurs. Most MCAs are equipped with dead-time meters to record the amount of time that the system is busy processing signals so that a correction can easily be made.

In some counting applications, it is advantageous to reduce contributions due to unwanted background by counting only the events recorded in the photopeak. Photopeak or photofraction efficiency curves have been developed and are available in Knoll (1989), *Harshaw Scintillation Phosphors* (1975), and Birks (1964). This type of measurement is performed by setting a voltage window around the photopeak or region of interest. These measurements can be performed with a less-expensive electronic device called a *scaler*. A scaler simply records a count for each pulse that occurs between two voltage settings.

The geometric factor is addressed by using a crystal shape that improves the counting efficiency. Popular geometries include cylindrical end wells, cylindrical side wells, and stacking multiple detectors. Special rectilinear well geometries are also available. All well geometries cause degradation of the energy resolution; however, this is usually not a significant issue because the energy of the photon being measured is typically already known. For low-energy photons, counting efficiencies are improved by reducing the Z or the material thickness of the entrance window or the well liner. Thin sheets of either aluminum or beryllium are used often in planar counting applications.

e. Signal-to-Noise Ratio Issues

The SNR of a counting system is an important concern. Some applications have a limited signal available to be detected. This is true in medical-imaging applications, in which the dose to the patient is an important consideration. Good measurements require a good SNR. Each measurement requires an analysis in which an acceptable confidence level has been established. If the optimal signal strength or count rate is achieved, then the noise must be reduced to ensure an acceptable SNR. This section discusses some of these noise issues.

First, it must be understood that the radioactive decay process is random. The time between radioactive decay events cannot be predicted. Only the statistics of the next event can be stated. Because of the random nature of the radioactive decay process, the statistics of radiation measurement counting must be understood.

Sources of noise from the detector assembly include the scintillator, detector hardware, PMT, and the voltage divider assembly. Noise contributed by the scintillator can include any parameter that causes the PHR to degrade: intrinsic background due to radioactive impurities, Compton scattering from surrounding materials, and any background radiation present such as terrestrial or cosmic radiation.

The PHR directly affects the SNR in photofraction measurements because, as the energy window widens to include all the events in the photopeak, more background events from the Compton continuum are also included in the same counting window. The background from impurities can be limited by using cleaner starting materials during growth of the ingot. Background from surrounding materials can be limited by improving the shielding around the detector. In multiple-detector counting systems, Compton scatter or cross-talk between detector elements can be minimized with lead or tungsten septa.

The PMT also contributes to the noise in the counting system. One form of PMT noise is called dark current. When a PMT is operated in the dark, it still exhibits some amount of current at the anode. One contributor to dark current is thermionic noise, which is a result of the very low work functions of the photocathode and the dynode surfaces. Other sources of dark current include leakage current between the anode and other electrode surfaces, leakage current between the PMT leads at the surface of the glass envelope, and scintillation events in the PMT glass. Another source of PMT noise is improperly selected PMT glass that has a high concentration of potassium. The ^{40}K present increases the background noise in the detector.

PMT's can also add to the noise problem by degrading the PHR. This occurs with excessive photocathode nonuniformity, poor linearity, or poor stability because of long- or short-term drift. Improper voltage-divider design or assembly can also lead to electronic noise.

Many of the problems discussed here are component design issues and can be resolved by better component engineering. Some of the noise problems discussed here can be minimized with the appropriate counting system design, such as good shielding, gain stabilization techniques, and even a Compton suppression detector configuration; other sources of systematic noise can be reduced by spectral stripping techniques, such as background subtraction.

3. Detector Configurations in Measurement System Applications

Applications for scintillation detectors include nuclear medicine, dose calibration, health physics, whole-body counting, meteorology, oil and gas exploration, uranium exploration, precious mineral exploration, biology, archeology, food research, high-energy particle physics, environmental air and soil monitoring, water analysis, commercial density gauging, snow-pack analysis, nuclear power, space exploration, academic research, isotopic characterization, drug interdiction, nuclear weapons compliance verification, and portal monitors. This section discusses the common detector configurations and some special detector designs. The detector configurations discussed here are produced in many sizes and shapes. Some are designed to withstand extreme environmental conditions that require special ther-

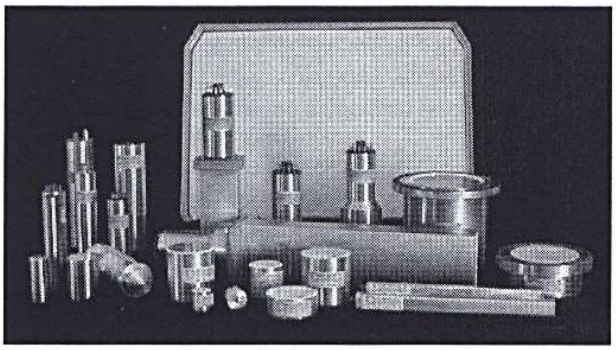

FIGURE 20 Photograph of various scintillation detectors. (Photo courtesy of Alpha Spetra, Inc.)

mal and mechanical designs. The discussion demonstrates the range of capabilities of detector technology. An assortment of scintillation detectors is shown in Figure 20.

a. Simple Gross Counters

Simple gross-counting detectors are usually open-face or integral-type units that do not require good resolution. The integral type is constructed with a PMT, whereas the open-face type is supplied with an optical window. Gross-counting units are used in many field applications in which damage to the PMT or crystal can easily occur. With a demountable PMT, either the crystal or the PMT can easily be replaced without incurring the cost of replacing both components. Gross counting measurements are done by setting a lower-energy threshold (discriminator) and counting all the pulses that take place without recognizing the pulse height. Gross counters do not perform spectroscopy. Sometimes gross counters employ energy windows that are set up to measure a particular gamma-ray of interest.

b. Well Counters

Well counters are detectors that have end, side, or through holes bored into the crystal. For an example of a well detector, see Figure 17. Well detectors are designed to improve 4π counting efficiency. Wells can be machined in numerous shapes to accommodate the end-user's requirements. Well counters are used as dose calibrators, environmental sample measurements, and other applications in which good counting efficiency is required.

c. Thin Windows

Thin window assemblies are designed to detect low-energy photons between 5 and 100 keV. The detector crystal is usually a thin section of 1–2.5-mm in thickness. These thin sections are optimal for detecting photons at low energies. At the same time, the detection of Compton scattered photons from higher energies is minimized. Thin window detectors use low-Z entrance windows to enhance counting efficiency. Some NaI(Tl) thin windows use cleaved crystal material to eliminate the dead layer associated with the process of machining and polishing a crystal. A cleaved crystal is more sensitive to low-energy X-rays.

A very popular thin window configuration, a F.I.D.L.E.R. (field instrument for the detection of low-energy radiation) probe, uses a 5-in-diameter by 0.063-in-thick NaI(Tl) crystal with a 0.010-in-thick beryllium entrance window. This unit is very useful in measuring the very low energy (~15 keV) characteristic of L-shell X-rays.

d. Low-Background Counting Assemblies and Compton Suppression Counting

Some applications, such as measuring environmental air samples, activation analysis, tracing contaminants, and measuring low-count-rate branching ratios (Cecil and Wilkinson, 1984), require the capability of measuring activities that are less than the ambient background! Low background counting systems can be designed to measure either external or internal source samples. This discussion focuses on measuring internal samples that can be placed inside the detection assembly.

There are several methods of obtaining the best possible lower limit of detection (LLD). These counting techniques can easily improve the SNR by an order of magnitude. The first approach to measurements such as this is to reduce as much of the background from the detector assembly as possible by special construction techniques. The low background detector assembly is then placed in a lead-lined (sometimes up to 4 inches of lead) enclosure to reduce signal from ambient background. In addition, lead shields are sometimes copper-lined to reduce the contribution from gamma-ray interaction with the lead and causing X-ray background.

The second approach uses an annular detector that surrounds the main plug detector, usually a HPGe (hyper-pure germanium) solid-state-type detector. The plug detector is situated in an axial well of the annular detector and is shielded from background radiation by the annular detector and by surrounding lead shielding. The annular detector, which can be made from NaI(Tl) or BGO, acts as passive shield. A BGO annulus is more compact due to its higher density; this reduces the size and amount of shielding that is required.

There are three popular methods of using annular detectors: Compton suppression by the anticoincidence counting mode, the sum coincidence mode, and the pair spectrometer mode. The anticoincidence counting system rejects pulses that are coincident in both the main detector and the annular detector by electronically gating the signals in such a way that only the remaining pulses registered in the main detector are accepted. The disadvantage of this technique is that, in some counting experiments in which a nuclear transition has coincident events, a good signal is sometimes rejected. This

technique has recently been used to measure the total electron energy resolution of a scintillation detector (Mengesha and Valentine, 1999).

The sum coincidence mode requires that an event occur in both the main detector and the annulus in coincidence in order to be accepted. This technique is effective because most of the Compton continuum spectrum is composed of single Compton scattering events followed by the escape of the scattered gamma-ray. Photopeak events consist of multiple scatters followed by a photoelectric absorption. In both instances, the events can be shared by the main detector and the surrounding annulus. The peak-to-Compton ratio can be improved if the counting system requires multiple scattering events to occur before an event is accepted. In practice, this is done by segmenting the detectors and gating the coincidence signal on all of the segments.

The pair spectrometer mode is only used in applications in which the gamma-ray energy is sufficient to cause pair production. This technique requires that three events be measured in coincidence: each annihilation photon created should be registered in opposite segments of the annular detector and the remaining energy of the incident photon, the second escape peak, should be counted in the main detector. This technique is very effective at eliminating cosmic-ray background; however, the detection efficiency in this technique is very poor.

e. Whole-Body Counting

Another low-background counting application is a whole-body counter. Workers that handle radioactive materials are frequently tested to assess the possibility of ingestion or inhalation of radioactive contamination. The detectors are placed in a room designed to provide a low-background counting environment. Several large-volume NaI(Tl) detectors of over 4000 cc each are positioned along the torso. The signals from all of the detectors are summed together. The data can also be stored so that additional analysis can provide information about the region of the body that may be exhibiting an abnormally high count rate. More recently, NaI(Tl) detectors have been used to screen workers while HPGe detectors are used to provide follow-up measurements.

f. Phoswich Measurements

Scintillators of different materials can be optically coupled and then interfaced to a PMT to form a phoswich, or phosphor sandwich as it was originally called (Mayhugh *et al.*, 1978). This combination is useful because events that occur in each crystal material can be separated by pulse-shape discrimination (Birks, 1964; Wilkinson, 1952) because of the different decay times. NaI(Tl) and CsI(Na) are commonly used in this configuration. This is especially useful when a low-energy particle or photon can be absorbed fully in the first scintillator while the more penetrating higher-energy photons are detected in the second scintillator.

g. Ruggedized High Temperature

One of the more demanding applications for scintillation detectors is the geophysical measurement done in borehole logging. Some measurements are actually taken while the borehole tool is drilling through rock formations. Thermal shock, mechanical shock, and severe mechanical vibration to the detector and PMT are the challenges that the design engineer must face. Because the borehole environment is cylindrical, the detector geometry is cylindrical with a typical aspect ratio of approximately 4:1. Energy resolution is sacrificed in this application because light output is not optimized at these aspect ratios.

h. Timing Resolution

The moment at which the incident radiation is absorbed by the scintillator and the light pulse is created is well defined. The time between pulses can easily be resolved to several nanoseconds by using a scintillation material that has a fast decay time, a crystal that is properly sized, photomultiplier tubes that have fast rise times, and good pulse-counting electronics. This technique is useful in high-count-rate applications and coincident gamma counting in PET. This technique can be used to determine the annihilation-photon time of flight (TOF) with proper electronics.

i. Gain Stabilization Techniques

In measurement situations where temperature fluctuations are encountered, gain stabilization techniques called pulsers can be used. A pulser may be either an electronic device such as a light-emitting diode or a radioactive source (an ^{241}Am pulser) that is intentionally incorporated into the detector assembly. In either approach, the light pulse measured by the counting system is situated in the spectrum so that it does not interfere with the region of interest in the spectrum.

4. Medical Imaging Applications

The most extensive use of scintillation detectors is in nuclear medicine. Table 6 gives a list of the most commonly used scintillation materials in medical applications. The detectors have been used in numerous medical applications including isotope preparation, studies of biological samples, anatomical studies, whole-body counting, *in vivo* counting, and body-function studies. By far the greatest use is in imaging anatomical regions of the body.

Three types of devices are briefly discussed in this section: the Anger Camera or gamma camera, PET, and *in vivo* probes. The detectors used are of many different sizes and shapes and include some of the most difficult to fabricate. Since the 1950s, vast improvements have been made in detector technology and measurement techniques used in nuclear medicine. More recently, software

Table 6 Crystal materials commonly used in medical applications

Material	Applications	Advantages	Disadvantages
NaI(Tl)	Gamma cameras, SPECT, PET, probes, dose calibrators	Light output, cost	Fragile, hygroscopic
BGO	PET	Density	Light output
$CdWO_4$	CT	Density, low afterglow	Decay time
LSO	PET	Light output, density, decay time	Cost, intrinsic radio-active background

developments have significantly improved the performance of the measurement devices.

Each of these clinical measurement techniques requires that a radioactively labeled substance be injected into the patient's body. By carefully positioning the detector, it is used to measure the location and intensity of the tracer that is concentrated in the organ of interest. The ongoing challenge is to precisely image very small concentrations of radioactive tracer.

a. The Anger Camera—Single-Photon Emission Computed Tomography

The first scintillation camera or gamma camera proposed by Hal Anger (1957) consisted of a single-pinhole collimator, a 4-in-diameter by 1/4-in-thick NaI(Tl) crystal, seven 1.5-in PMTs, pulse-processing electronics, and an oscilloscope. The image was recorded with a Polaroid-Land camera. A later version of the basic Anger camera is shown in Figure 21. In his first paper, Anger reported the use of the counting apparatus in a clinical thyroid study; the immediate advantage seen over the existing scanning technology was the shorter imaging time.

Currently, gamma camera counting systems can have as many as three large field of view camera heads that have the capability of acquiring data while in motion. Currently available systems have the ability to take data over 360° and over multiple planes. Today SPECT systems are equipped with analog-to-digital convertors (ADCs) for signal processing. Computers are used to manipulate data during image reconstruction, store the data, and display the image. Typical spatial resolution is approximately 4 mm. Most studies are performed using ^{99m}Tc, which emits a 140-keV gamma ray.

Improvements in gamma camera technology are aimed at improving the spatial resolution, sensitivity, and uniformity of response as seen in the image. New hardware and software developments are continually being reviewed to improve the performance of gamma camera systems.

b. Positron Emission Tomography

The basis for PET is the coincident measurement of the 511-keV photons (created during positron annihilation) by a multi-element array of scintillation detectors. The first PET detector array built for tomographic imaging was the Brookhaven National Laboratory BNL-32 (Robertson *et al.*, 1972: Yamamoto, 1977). The BNL-32 crystal positron transverse section detector was built in 1972. Another early PET system was built with NaI(Tl) crystals in 1973 by Phelps *et al.* (1975). Soon after, the first BGO crystals were used because they are much more dense than NaI(Tl) crystals; this helped improve the system detection efficiency. More recently, LSO is being used due to its better light output and slightly higher density. With each generation of PET imaging device, the number of detector elements has increased. The current high-resolution research tomograph (HRRT) has approximately 120,000 pixelated elements (Schmand, 2000).

A schematic for a simple PET system is shown in Figure 22. A positron-emitting radioisotope is injected into the patient. The subsequent emission of the 511-keV photons is detected by two opposing detectors. The signals are processed and an image is reconstructed from the digitized data.

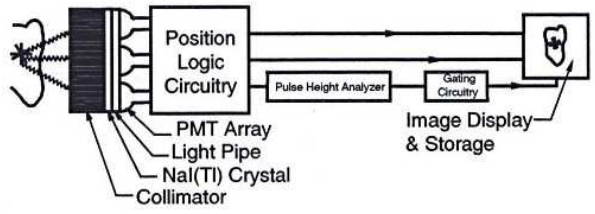

FIGURE 21 The basic Anger camera.

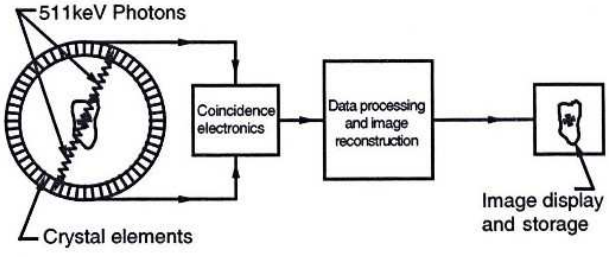

FIGURE 22 PET imaging system.

Recently a hybrid PET/SPECT instrument has been developed (Schmand, 2000), which incorporates NaI(Tl) to function in the SPECT modality and LSO to function in the PET modality.

c. In Vivo *Measurements*

In vivo counting systems are used to detect radioactivity that has been injected into the patient. Typically a single-element device, the *in vivo* probe measures a specific organ or anatomical region. Applications include a system for measuring thyroid uptake, cardiac studies, pulmonary studies, and surgical probes. Surgical probes are specifically designed to aid the physician in detecting cancerous tissue during surgery.

VI. SUMMARY AND COMMENTS

What will be the next improvement in scintillator technology? It seems that the initiative to develop new scintillators comes mainly from the medical imaging community and the high-energy physics community (Lecoq, 1999; Korzhik and Lecoq, 2000, 2001). We should recall the discussion regarding the ideal scintillator and how the technology has progressed (Heath *et al.*, 1979; Weber, 1999). The research community has developed some ingenious approaches in the search to find new scintillators (Derenzo *et al.*, 1990, 1994; Moses and Derenzo, 1990; Melcher and Schweitzer, 1992; Balcerzyk *et al.*, 2000). Unfortunately, at this time, the performance of any new potential materials cannot be predicted from theory.

Many useful materials have been developed since the 1950s; however, none performs well enough to completely replace NaI(Tl). There is a need for improvement in the crystal-growth techniques that are currently used. There is a need to improve the performance of light collection devices. There are numerous research projects in process with the continued hope of developing a much-improved scintillator material. A number of Ce-doped compound scintillators are currently being developed, and they show some promise due to improved speed and energy resolution. Examples include $LaBr_3(Ce^{3+})$, $LaCl_3(Ce^{3+})$, $K_2LaCl_3(Ce^{3+})$, and $RbGd_2Br_7(Ce^{3+})$. $LaBr_3(Ce^{3+})$ in very small pieces has demonstrated a PHR of approximately 3.3% at 662 keV, whereas both $K_2LaCl_3(Ce^{3+})$ and $RbGd_2Br_7(Ce^{3+})$ have demonstrated a PHR of approximately 4% at 662 keV (van Loef *et al.*, 2001). As with many other scintillators being developed, much work needs to be done with these materials to improve them until they become commercially available in large pieces and large quantities.

In this chapter, we have seen that scintillation detector technology uses many different skills and expertise: physics, chemistry, material science, thermodynamics, nuclear physics, quantum mechanics, solid-state physics, optics, mechanical engineering, electronic engineering, mathematics and statistics, and computing. Good detector design and fabrication require cooperation between experts in several scientific and engineering disciplines. For these reasons, the author has enjoyed working with scintillation detectors for over 25 years.

The word scintillation comes from the Latin verb *scintillare,* which means to sparkle or glitter. Consider this thought: The very small amount of light given off by a crystal has the ability to provide many useful tools, yet at the same time this light is lost to the human eye!

It is true that out of a little light there is much to be profited.

References

Anger, H.O. (1957). Scintillation camera. *Rev. Sci. Instrum.* **29:** 27–33.

Balcerzyk, M., Moszynski, M., Kapusta, M., Wolski, D., Pawelke, J., and Melcher, M., (2000). YSO, LSO, GSO and LGSO. A study of energy resolution and nonproportionality, *IEEE Trans. Nucl. Sci.* **47:** 1319–1324.

Beattie, R.J.D., and Byrne, J. (1972). A Monte Carlo program for evaluating the response of a scintillation counter to monoenergetic gamma rays. *Nucl. Instrum. Methods* **104:** 163–165.

Birks, J. B. (1964). "The Theory and Practice of Scintillation Counting," Pergamon Press, The MacMillan Company, New York.

Cecil, F.E., and Wilkinson, F.J. (1984). Measurement of the ground state gamma-ray branching ratio of the dt reaction at low energies. *Phy. Rev. Lett.* **53:** 767–770.

The Crystal Ball Collaboration. (1980). "A Brief Review of Recent Results from the Crystal Ball at SPEAR," SLC-PUB-2655, Nov. 20.

Derenzo, S.E., Klintenberg, M.K., and Weber, M.J. (1999). Quantum mechanical cluster calculations of critical scintillation processes. *Proceedings of the Fifth International Conference on Inorganic Scintillators and Their Applications.* p. 53–60.

Derenzo, S.E., Moses, W.W., Weber, M.J., and West, A.C. (1994). Scintillator and phosphor materials. *Mat. Res. Soc. Symp. Proc.* **348:** 39–49.

Derenzo, S.E., *et al.* (1990). Prospects for new inorganic scintillators. *IEEE Trans. Nucl. Sci.* **37:** 203–208.

Derenzo, S.E., *et al.* (2000). Measurements of the intrinsic rise times of common inorganic scintillators. *IEEE Trans. Nucl. Sci.* **47:** 860–864.

Dorenbos, J.T., de Haas, J.T.M., and van Eijk, C.W.E. (1975). Nonproportionality in the scintillation response and the energy resolution obtainable with scintillation crystals. *IEEE Trans. Nucl. Sci.* **42:** 2190–2202.

Eby, F., Jentschke, W., (1954). Fluorescent response of NaI(Tl) to nuclear radiations. *Phys. Rev.* **96:** 911.

Evans, R. D. (1955). "The Atomic Nucleus," McGraw-Hill, New York.

Fonte, R., Insolia, A., Lanzano, G., Pagano, A., Russo, G.V., Palama, G., de Jager, C.W., and de Vries, H. (1991). Response function of a BaF_2 detector to electrons. *Nucl. Instrum. Methods Phys. Res. A* **353:** 80–82.

Harshaw Scintillation Phosphors. (1975). Third Edition, (Company Catalog).

Harshaw, J.A., Stewart, E.C., and Hay, J.O. (1993). AEC Report NYO 1577, 1952. Preparation and Performance of Scintillation Crystals. *Research A* **333:** 304–311.

Harshaw Radiation Detectors. (1984). (Company Catalog).

Heath, R.L., Hofstadter, R., and Hughes, E.B. (1979). Inorganic scintillators, a review of techniques and applications. *Nucl. Instrum. Methods* **162:** 431–476.

Hendee, W.R. (1984). "Radioactive Isotopes in Biological Research," Krieger Publishing Company.

Hofstadter, R. (1948). Alkali halide scintillation counters. *Phys. Rev.* **74:** 100–101.

Hofstadter, R. (1975). Twenty-five years of scintillation counting. *IEEE Trans. Nucl. Sci.* **22:** 13–25.

Holl, I., Lorenz, E., and Mageras, G. (1988). A measurement of light yield of common inorganic scintillators. *IEEE Trans. Nucl. Sci.* **25:** 105–109.

Iredale, P. (1961). The effect of the non-proportional response of NaI(Tl) crystals to electrons upon the resolution for g-rays. *Nucl. Instrum. and Methods* **11:** 340–346.

Ishii, M. and Kobayashi, M. (1991). Single crystals for radiation detectors. *Prog. Crystal Growth and Characteristics* **23:** 245–311.

Knoll, G. F. (1989). "Radiation Detection and Measurement." John Wiley & Sons, New York.

Kobayashi, M., Carlson, P., and Berglund, S. (1989). Temperature dependence of CsI(Tl) scintillation yield for cosmic muons, 5 and 1.25 MeV γ-rays. *Nucl. Instrum. Methods Phys. Res. A* **281:** 192–196.

Kobayashi, M., Mitsuru, I., and Melcher, C. L. (1993). Radiation damage of a cerium-doped lutetium oxyorthosilicate single crystal. *Nucl. Instrum. Methods A* **335:** 509–512.

Korzhik, M., and Lecoq, P. (2001). Search of new scintillation materials for nuclear medicine application. *IEEE Trans. Nucl. Sci.* CD, article 6-1.

Korzhik, M., and Lecoq, P. (2000). Scintillator developments for high energy physics and medical imaging. 0-7803-5696-9/00. *IEEE Trans. Nucl. Sci.* **47:** N4, 1311.

Lecoq, P. (1999). How high energy physics is driving the development of new scintillators. *Proceedings of the Fifth International Conference on Inorganic Scintillators and Their Applications.* pp. 3–10

Lempicki, A., Wojtowicz, A.J., and Berman, E. (1993). Fundamental limits of scintillator performance. *Nucl. Instrum. Methods Phys. A* **333:** 304–311.

Mayhugh, M.R., Lucas, A.C., and Utts, B.K. (1978). Low background beta counting with CaF_2(Eu) in a Phoswich configuration. *IEEE Trans. Nucl. Sci.* **25:** 569–573.

Meggitt, G.C. (1970). The effect of the crystal surface on the derived electron scintillation response of NaI(Tl). *Nucl. Instrum. Methods* **83:** 313–316.

Melcher, C.L. (2000). Scintillation counters for PET. J. Nucl. Med. **41:** 1051–1055.

Melcher, C.L., Schweitzer, J.S. (1992). A promising new scintillator: cerium-doped lutetium oxyorthosilicate. *Nucl. Instrum. Methods Res. Phys. A* **314:** 212–214.

Mengesha, W., and Valentine, J.D. (1999). A technique for measuring scintillator electron energy resolution using a Compton coincidence technique. *Proceedings of the Fifth International Conference on Inorganic Scintillators and Their Applications.* pp. 173–178.

Moses, W.W. and Derenzo, S.E. (1990). Lead carbonate, a new fast heavy scintillator. *IEEE Trans. Nucl. Sci.* **37(2):** 96–100.

Murray, R.B. (1975). Energy transfer in alkali halide scintillators by electron-hole diffusion and capture. *IEEE Trans. Nucl. Sci.* **22:** 54–57.

Narayan, G.H., and Prescott, J.R. (1968). The contribution of the NaI(Tl) crystal to the total linewidth of NaI(Tl) scintillation detectors. *IEEE Trans. Nucl. Sci.* **15:** 162–166.

Branch, Uber, J., Smyth, K., and Walch, C. (1980). NASA Interoffice Communication, Materials Control and Applications Branch. "MOR Bend Test results for NaI(Tl) and Additional Elastic Moduli Measurements."

Phelps, M.E., and Hoffman, E.J., Mullani, N.A., Ter-Pogossian, M.M. (1975). Application of annihilation coincidence detection to transaxial reconstruction tomography. *J. Nucl. Med.* **16:** 210–224.

Prescott, J.R. and Narayan, G.H. (1969). Electron response and intrinsic line-widths in NaI(Tl). *Nucl. Instrum. Methods* **75:** 51–55.

Robbins, D.J. (1980). On predicting the maximum efficiency of phosphor systems excited by ionizing radiation. *J. Electrochem. Soc.* **127:** 2694–2702.

Robertson, J.S., *et al.* (1972). In "Tomographic Imaging in Nuclear Medicine" (G.S. Freedman, ed.) pp. 142–153. The Society of Nuclear Medicine, Inc., New York.

Rodnyi, P. A. (1997). "Physical Processes in Inorganic Scintillators," CRC Press, Boca Raton, FL.

Sakai, E. (1987). Recent measurements on scintillator-photdetector systems. *IEEE Trans. Nucl. Sci.* **NS34:** 418–422.

Schmand, M. (2000). "Higher Resolution PET by Means of a New Scintillator LSO," Ph.D. thesis, Max-Planck-Institute for Neurological Research.

Schweitzer, J.S., and Ziehl, W. (1983). Temperature dependence of NaI(Tl) decay constant. *IEEE Trans. Nucl. Sci.* **NS30:** 380.

Snyder, R.S., and Clotfelter, W.N. (1974). NASA Technical Memorandum, NASA TM X-64898, Physical Property Measurements of Doped Cesium Iodide Crystals. George C. Marshall Space Flight Center, Alabama.

Sorenson, J.A., Phelps, M.E. (1987). "Physics in Nuclear Medicine," W.B. Saunders Company, New York.

Tidd, J.L., Dabbs, J.R., and Levine, N. (1973). NASA Technical Memorandum, NASA TM X-64741. Scintillator Handbook with Emphasis on Cesium Iodide. George C. Marshall Space Flight Center, Alabama.

Valentine, J.D., Wehe, D.K., Knoll, G.F., Moss, C.E. (1993). Temperature dependence of CsI(Tl) absolute scintillation yield. *IEEE Trans. Nucl. Sci.* **40:** 1267–1274.

Valentine, J.D., and Rooney, B.D. (1994). Design of a compton spectrometer experiment for studying scintillator non-linearity and intrinsic energy resolution. *Nucl. Instrum. Methods Phys. Res. A* **353:** 37–40.

van Eijk, C.W. (2000). Inorganic-scintillator development. *Nucl. Instrum. Methods A* **460:** 1–14.

van Loef, E.V.D., *et. al.* (2001). High-energy-resolution scintillator: Ce^{3+} activated $LaBr_3$. *Appl. Phys. Lett.* **79:** 1573–1575.

Weber, M.J. (1999). "Inorganic Scintillators Today and Tomorrow." IEEE Symposium Presentation, Lawrence Berkeley National Laboratory.

Wilkinson, D.H. (1952). The Phoswich-A multiple phosphor. *Rev. Sci. Instrum.* **23:** 414.

Yamamoto, Y.L. (1977). Dynamic position emission tomography for study of cerebral hemodynamics in a cross section of the head using positron-emitting ^{68}Ga-EDTA and ^{77}Kr. *J. Comput. Assis. Tomogr.* **1(1):** 43–56.

Zerby, C.D., Meyer, A., and Murray, R.B. (1961). Intrinsic line broadening NaI(Tl) gamma-ray spectrometers. *Nucl. Instrum. Methods* **12:** 115–123.